Deep posteromedial cortical rhythm in dissociation

https://doi.org/10.1038/s41586-020-2731-9

Received: 5 November 2019

Accepted: 20 August 2020

Published online: 16 September 2020

Check for updates

Sam Vesuna[1,8], Isaac V. Kauvar[1,2,8], Ethan Richman[1], Felicity Gore[1,7], Tomiko Oskotsky[1,3], Clara Sava-Segal[4], Liqun Luo[5,6], Robert C. Malenka[7], Jaimie M. Henderson[3], Paul Nuyujukian[1,2,3], Josef Parvizi[4] & Karl Deisseroth[1,6,7] ✉

Advanced imaging methods now allow cell-type-specific recording of neural activity across the mammalian brain, potentially enabling the exploration of how brain-wide dynamical patterns give rise to complex behavioural states[1–12]. Dissociation is an altered behavioural state in which the integrity of experience is disrupted, resulting in reproducible cognitive phenomena including the dissociation of stimulus detection from stimulus-related affective responses. Dissociation can occur as a result of trauma, epilepsy or dissociative drug use[13,14], but despite its substantial basic and clinical importance, the underlying neurophysiology of this state is unknown. Here we establish such a dissociation-like state in mice, induced by precisely-dosed administration of ketamine or phencyclidine. Large-scale imaging of neural activity revealed that these dissociative agents elicited a 1–3-Hz rhythm in layer 5 neurons of the retrosplenial cortex. Electrophysiological recording with four simultaneously deployed high-density probes revealed rhythmic coupling of the retrosplenial cortex with anatomically connected components of thalamus circuitry, but uncoupling from most other brain regions was observed—including a notable inverse correlation with frontally projecting thalamic nuclei. In testing for causal significance, we found that rhythmic optogenetic activation of retrosplenial cortex layer 5 neurons recapitulated dissociation-like behavioural effects. Local retrosplenial hyperpolarization-activated cyclic-nucleotide-gated potassium channel 1 (HCN1) pacemakers were required for systemic ketamine to induce this rhythm and to elicit dissociation-like behavioural effects. In a patient with focal epilepsy, simultaneous intracranial stereoencephalography recordings from across the brain revealed a similarly localized rhythm in the homologous deep posteromedial cortex that was temporally correlated with pre-seizure self-reported dissociation, and local brief electrical stimulation of this region elicited dissociative experiences. These results identify the molecular, cellular and physiological properties of a conserved deep posteromedial cortical rhythm that underlies states of dissociation.

Recent advances in large-scale high-speed recording and control of neuronal activity have enabled exploration of natural and causal neural-circuit dynamics spanning the mammalian brain. We considered that these technological advances constitute a newly emerged opportunity to explore the cellular implementation of altered behavioural states that might require a global perspective to understand. Dissociation represents a paradigmatic example of such a state.

In dissociation—which can be elicited by diverse causes including stress, epilepsy, dissociative drugs or certain neuropsychiatric disorders—the normal integration of cognitive processing is disrupted. A selective uncoupling can be observed, in which affective or emotional responses are dissociated from sensory percepts, and the sense-of-self is dissociated from body position or action. However, despite its substantial basic and clinical importance, the underlying cellular and circuit mechanisms of dissociation remain unknown. Here we investigate the dissociative-like behavioural state using high-speed, brain-wide approaches in both mice and humans, and identify underlying deep posteromedial-cortex rhythmic dynamics along with molecular, cellular and physiological mechanisms.

Imaging reveals a retrosplenial rhythm

We recorded multiregional neuronal activity using widefield macroscopy, a cleared skull preparation, and atlas registration in mice expressing GCaMP6s[6,8,15] (Fig. 1a–c). Upon intraperitoneal injection of ketamine (50 mg kg^{-1}, a subanaesthetic dose; see Methods), a 1–3-Hz oscillation

[1]Department of Bioengineering, Stanford University, Stanford, CA, USA. [2]Department of Electrical Engineering, Stanford University, Stanford, CA, USA. [3]Department of Neurosurgery, Stanford University, Stanford, CA, USA. [4]Department of Neurology and Neurological Sciences, Stanford University, Stanford, CA, USA. [5]Department of Biology, Stanford University, Stanford, CA, USA. [6]Howard Hughes Medical Institute, Stanford University, Stanford, CA, USA. [7]Department of Psychiatry and Behavioral Sciences, Stanford University, Stanford, CA, USA. [8]These authors contributed equally: Sam Vesuna, Isaac V. Kauvar. ✉e-mail: deissero@stanford.edu

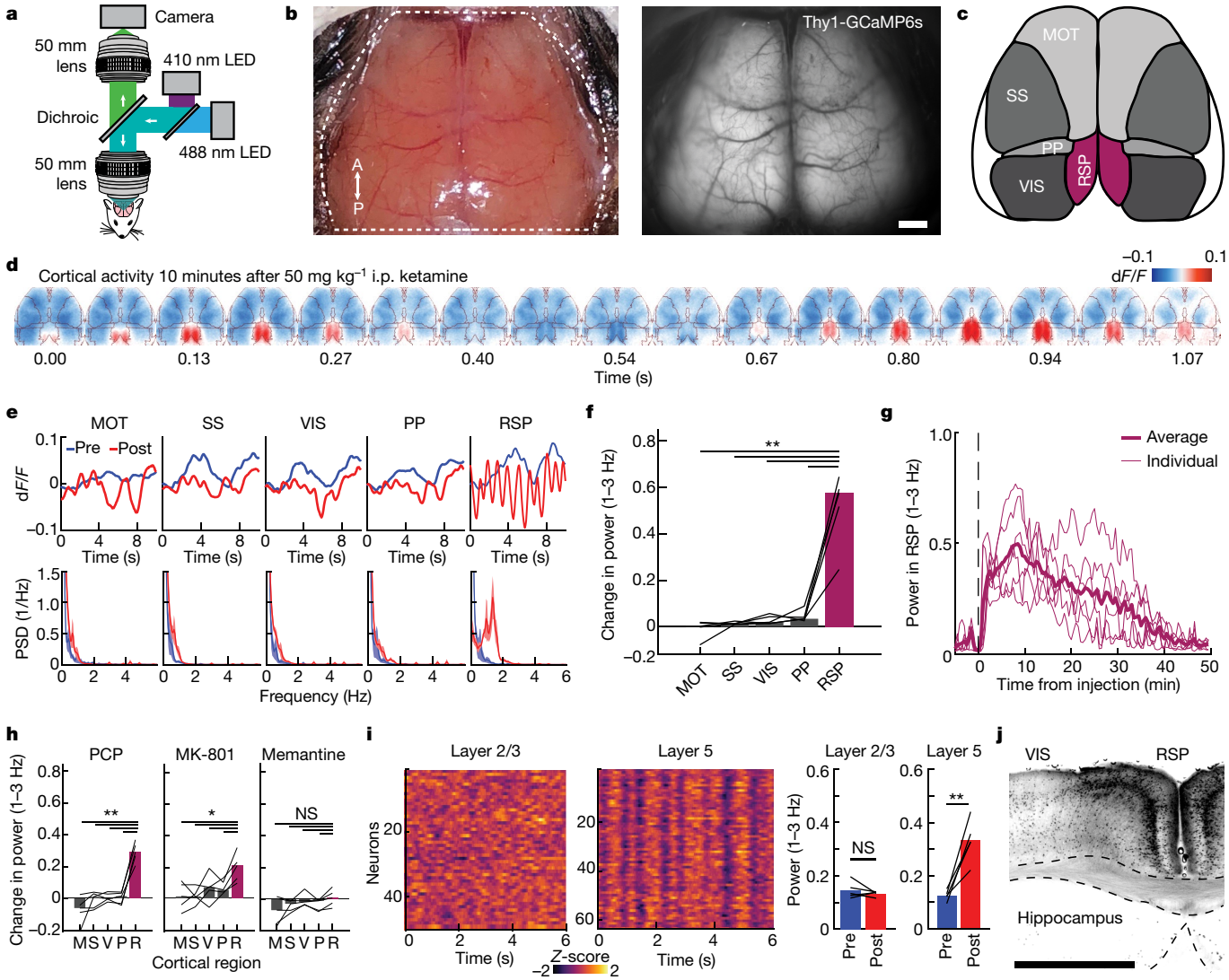

Fig. 1 | Multiregional widefield imaging of cortical activity reveals ketamine-induced retrosplenial rhythm. a, Schematic of the widefield macroscopy setup. **b**, Left, transparent skull preparation; right, 488-nm-excited fluorescence image from a Thy1-GCaMP6s mouse. A, anterior; P, posterior. Scale bar, 1 mm. **c**, Neocortex atlas for alignment. MOT, motor; SS, somatosensory; PP, parietal; VIS, visual; RSP, retrosplenial. **d**, Cortical activity, visualized by a video sequence of 410-nm-corrected fluorescence over 1 s, in a Thy1-GCaMP6s mouse 10 minutes after i.p. injection of 50 mg kg^{-1} ketamine. RSP activation is observed at 0.13 s and 0.8 s; deactivation at 0.54 s. dF/F scale is normalized by median fluorescence intensity. **e**, Top, fluorescence traces from five regions before (blue) and 10 min after (red) injection of 50 mg kg^{-1} ketamine. Shown are the 10-s, 410-nm-corrected data. Bottom, corresponding power spectral density (PSD) plots, obtained at minutes 10–11 post-injection (data are mean ± s.e.m.; $n = 5$ mice). **f**, Change in power of the 1–3-Hz rhythm after injection of ketamine, $n = 5$ mice, each black line represents a mouse. One-way ANOVA, repeated measures, $F_{4,16} = 25.4$, $P < 1 \times 10^{-4}$. Corrected two-sided paired t-tests, $^{**}P < 0.01$. Hedge's g effect sizes = 3.96, 3.90, 3.76, 3.62. **g**, Power at 1–3 Hz in the RSP over 55 min, obtained from widefield imaging of GCaMP6s, with 50 mg kg^{-1} ketamine injected intraperitoneally 5 min into recording. The thick trace shows the mean for $n = 6$ mice. **h**, Change in power of the 1–3-Hz rhythm after administration of PCP, MK801 and memantine. The mean power at 1–3 Hz is shown ($n = 5$ mice per drug). Corrected two-sided paired t-tests, $^{*}P < 0.05$, $^{**}P < 0.01$, NS (not significant) $P > 0.05$. Hedge's g effect sizes: PCP = 4.23, 4.57, 5.14, 4.87; MK801 = 1.80, 1.79, 2.16, 1.28, 1.56; memantine = 1.00, 0.96, 0.27, 0.82. **i**, Left, single-cell activity traces obtained from two-photon microscopy from layer 2/3 or layer 5 RSP after ketamine injection. Right, mean power of the 1–3-Hz rhythm across cells before and after ketamine administration. Layer 2/3, $n = 5$ mice, two-sided paired t-test, $P = 0.74$, Hedge's g effect size = −0.46. Layer 5, $n = 5$ mice, two-sided paired t-test, $P < 0.01$, Hedge's g effect size = 3.16. **j**, tdTomato fluorescence after recombination of TRAP2;Ai14 mice, after injection of 50 mg kg^{-1} ketamine, showing dense labelling of layer 5 cells. Dark cells are those expressing tdTomato. Scale bar, 1 mm.

emerged in the retrosplenial cortex (RSP), but not in any other cortical region (Fig. 1d–f, Extended Data Fig. 1a, Supplementary Video 1; $n = 5$ mice). The rhythm emerged within 120 s, returned to baseline after approximately 45 min (Fig. 1g, Extended Data Fig. 1b–e), and was similar in magnitude across five consecutive days; no ketamine-induced 1–3-Hz movements were observed (Extended Data Fig. 1g–i). Subanaesthetic ketamine reduced correlations between RSP activity and activity in all other dorsal-cortical regions (Extended Data Fig. 1j). We then used high-magnification two-photon microscopy to image superficial neuropil through a glass-covered cranial window, and observed the oscillation in the RSP but not in the neighbouring visual cortex (Extended Data Fig. 1k–o, Supplementary Video 2; $n = 4$ mice, paired t-test, $P = 0.035$).

In humans, ketamine can cause dissociation, analgesia, hallucinations, sedation and anaesthesia. To test whether other drugs with or without dissociative properties elicited similar cortical activity patterns, we repeated the imaging studies using N-methyl-D-aspartate (NMDAR) antagonists, a hallucinogen, anaesthetics, a sedative and an analgesic. Phencyclidine (PCP)—which, like ketamine, is a dissociative NMDAR antagonist—induced the RSP-localized oscillation (Fig. 1h), as did dizocilpine (MK-801), a long-lasting dissociative NMDAR-antagonist.

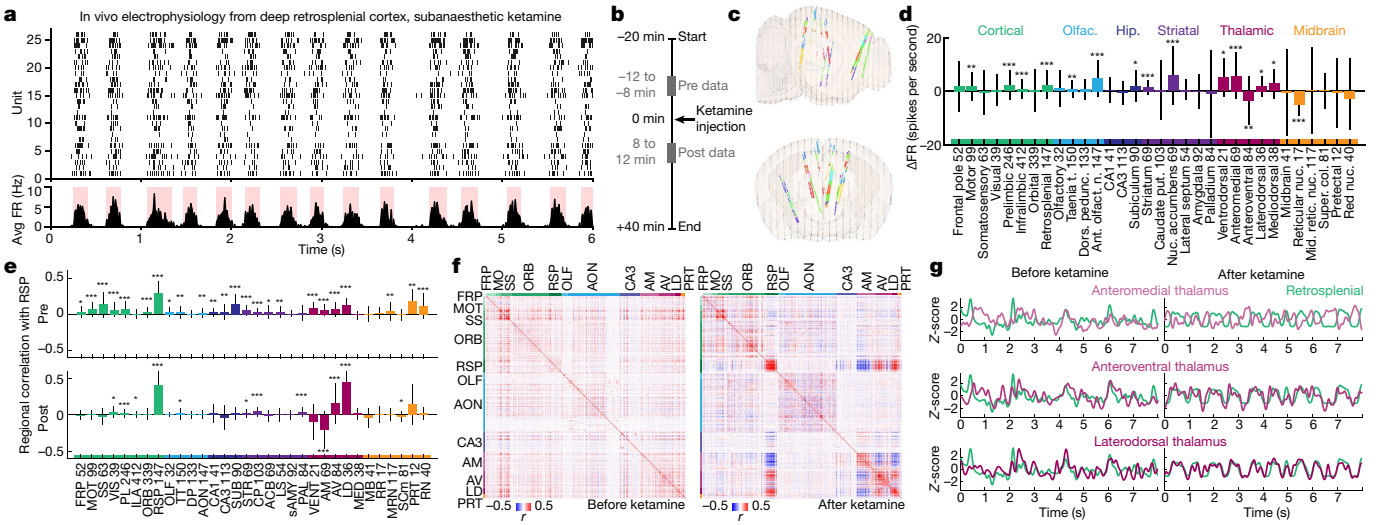

Fig. 2 | Retrosplenial in vivo electrophysiology. a, Top, spike-train rasters from all simultaneously recorded single units from the deep RSP in a head-fixed mouse after injection of a sub-anaesthetic dose of 50 mg kg^{-1} ketamine. Bottom, average firing rate (FR) of the units shown above (in Hz, 10-ms bin). The pink boxes indicate ON-states for bursts (see Methods). **b**, Timeline for a multi-Neuropixel recording session. Ketamine was injected i.p. 20 min into the recording session through a previously implanted cannula. **c**, 3D-reconstruction showing the insertion of Neuropixel probes (16 probe insertions are shown in total for 4 sessions). The different areas of the brain are shown by the changing colours along each probe. Four Neuropixels were implanted into each mouse and recorded simultaneously. **d**, Average change in firing rate per region between 8–12 min before and 8–12 min after ketamine injection. Cells from all four sessions were included. The number of units for each region is shown along the *x* axis, after the region name. Data are mean ± s.e.m. Corrected two-sided *t*-test versus 0, *$P < 0.05$, **$P < 0.01$, ***$P < 0.001$. Taenia t., taenia tecta; dors. pedunc., dorsal peduncular; ant. olfact. n., anterior olfactory nucleus; caudate put., caudate putamen; nuc. accumbens, nucleus accumbens; reticular nuc., reticular nucleus; mid. retic. nuc., midbrain reticular nucleus; super. col., superior colliculi; red nuc., red nucleus. **e**, Average RSP correlation (mean regional activity) before and after ketamine injection. The number of units for each region is shown along the *x* axis after the region names, which are stated as abbreviated forms of the names in **d**. Data are mean ± s.e.m. Corrected two-sided *t*-test versus 0, *$P < 0.05$, **$P < 0.01$, ***$P < 0.001$. **f**, Correlation matrix between cells, grouped by region before and after ketamine injection; obtained from 4-Neuropixel recordings in mouse. **g**, *Z*-scored mean activity traces (corresponding to rasters in Extended Data Fig. 7f) of three simultaneously recorded thalamic nuclei and RSP (green).

Memantine—a low-affinity, uncompetitive NMDAR-antagonist with a non-dissociative clinical profile—did not elicit the oscillation, nor did saline or lysergic acid diethylamide (LSD) (Extended Data Fig. 2). The non-dissociative anaesthetics dexmedetomidine and propofol, and a ketamine/xylazine cocktail that is frequently used in veterinary medicine, elicited waves of cortical activity that were not restricted to the RSP (Extended Data Fig. 3). Neither the GABAergic sedative diazepam nor the centrally acting opioid analgesic buprenorphine elicited the rhythm (Extended Data Fig. 4). Together, these data revealed an oscillatory pattern, spatially restricted to the RSP, that is selectively induced by dissociative agents.

The RSP rhythm is localized to layer 5 neurons

The multiregional imaging approach revealed spatially localized dynamics but did not enable the observation of layer-specific cellular contributions. We therefore restricted the expression of GCaMP6m to specific cortical layers and measured single-neuron Ca^{2+} signals in the RSP (Extended Data Fig. 5a, b). In layer 2/3 neurons (Cux2-CreER mice[16]), neither oscillating neurons nor population synchrony were observed (Fig. 1i, Extended Data Fig. 5c, d; $n = 5$ mice, paired *t*-test, $P = 0.7$). By contrast, layer 5 neurons (Rbp4-Cre mice[17]) exhibited synchronous activity (Fig. 1i, Extended Data Fig. 5e, f). We verified this layer specificity with brain-wide activity mapping using the TRAP2 mouse line[18,19]; layer 5 was specifically recruited (unpaired *t*-test, $P < 0.001$) (Fig. 1j, Extended Data Fig. 5g–i). Thus, under these conditions, ketamine elicited rhythmicity selectively in layer 5 RSP neurons.

Spiking pattern in the deep RSP and the thalamus

We extended our investigations to the single-spike millisecond-scale domain, obtaining electrophysiological recordings with 32-channel two-shank silicon probes. In mice injected with 50 mg kg^{-1} ketamine, deep RSP neurons engaged in intermittent synchronous bursts of around 250 ms, separated by silent states of around 250 ms (Fig. 2a, Extended Data Fig. 5j, k). Individual units fired about 5 to 10 spikes per burst; nearly all identified units participated in every burst event, and most bursts contained nearly all units, with structured temporal ordering (Extended Data Fig. 5l–p).

We then constructed a long-shank, high-contact-density recording system comprising four Neuropixels probes to simultaneously record hundreds of neurons throughout the brain (Fig. 2b, c, Extended Data Fig. 6a). Subanaesthetic doses of ketamine were found to influence several brain regions (Fig. 2d, Extended Data Fig. 6b, c). We observed the 1–3-Hz RSP rhythm as expected, but also discovered specific subcortical regions—inaccessible to cortical imaging—that exhibited increased rhythmicity (Extended Data Fig. 6d–g). Whereas nearly all brain regions were correlated with the RSP before the administration of ketamine, correlations were reduced 8–12 min after ketamine injection—notably in the somatosensory cortex, subiculum, ventral/anteromedial thalamus and the red nucleus (Fig. 2e, f, Extended Data Figs. 7a–e, 8).

A notable uncoupling was observed between adjacent, but differently connected, thalamic nuclei. Whereas the laterodorsal thalamus and the anteroventral thalamus (which have known posterior cortical wiring relationships, including to the RSP[20–22]) became more strongly correlated to each other and to the RSP, anteromedial thalamic neurons (which have known projections to the frontal cortex[20–22]) were found to oscillate out-of-phase with the RSP (Fig. 2f, g, Extended Data Fig. 7f–i). Brain-wide electrophysiology experiments therefore revealed a globally detectable activity-dissociation motif, which can be interpreted through the rhythm and the wiring of the RSP.

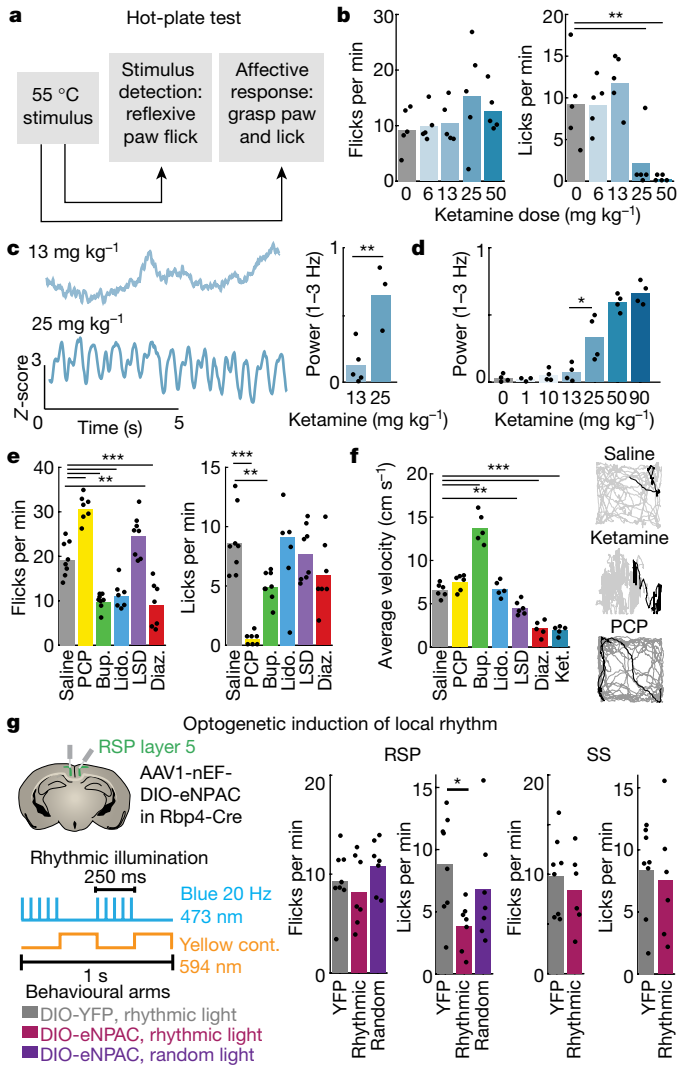

Fig. 3 | Ketamine- and optogenetically elicited dissociation-like behavioural phenotype. a, Stimulus detection (reflexive paw-flick) and affective/emotional response (protective paw-licking) during the hot-plate test. **b**, Rate of reflexive paw flicks (left) and licks (right) in ketamine-injected mice. One-way ANOVA with repeated measures: flick, $P = 0.38$; lick, $P = 5 \times 10^{-4}$. Corrected two-sided unpaired *t*-tests. $n = 5$ mice per group. For each dose in order, Hedge's *g* effect sizes for flick: 0.16, 0.26, 0.77, 0.77; and lick: −0.028, 0.53, −1.43, −2.19. **c**, Left, fibre photometry traces from RSP: the rhythm was observed at 25 mg kg^{-1} but not at 13 mg kg^{-1}. Right, 10 min after injection, the power at each dose across several mice ($n = 5$ mice for 13 mg kg^{-1}; $n = 3$ mice for 25 mg kg^{-1}; bars show mean values). Unpaired-*t*-test, $P = 0.008$, Glass's $\Delta = 3.2$. **d**, Mean power at 1–3 Hz as assessed by widefield imaging for different doses of ketamine, with 13 and 25 mg kg^{-1} doses statistically compared. $n = 4$ mice per dose, two-sided unpaired *t*-test, $^{*}P = 0.027$. **e**, Results of the hot-plate test after administration of drugs from other classes. Each experimental group is compared with the saline (control) group via a corrected Mann–Whitney *U*-test. For each drug in order, Hedge's *g* effect sizes: flick 3.10, −2.97, −2.19, 1.14, −2.16; Glass's Δ: lick −15.2, −2.89, 0.093, −0.40, −0.90. Corrected *P* values versus saline: flick 0.0001, 0.0001, 0.0008, 0.0297, 0.0008; lick 1.9×10^{-5}, 0.0092, 0.8146, 0.5761, 0.1395. Bup., buprenorphine; lido., lidocaine; diaz., diazepam. $^{**}P < 0.01$, $^{***}P < 0.001$. **f**, Left, average velocity of mice in the open-field test over a period of 5 min. Ketamine, LSD and diazepam decreased velocity, whereas buprenorphine increased velocity compared with controls. Each experimental group was compared with saline (control) via a corrected Mann–Whitney *U*-test. Hedge's *g* effect sizes: −6.14, 1.02, 4.98, 0.20, −2.34, −4.77. Corrected *P* values versus saline: 0.1021, 2.5×10^{-5}, 0.7206, 0.0020, 2.5×10^{-5}, 9.1×10^{-6}. Right, traces of body position during the open-field test after administration of saline or the stated dissociative drugs. The grey line shows the position of the mouse over the full 5-min session, whereas the black line shows the position over a 20-s tracking period, beginning in minute 2. **g**, Viral injections, illumination pattern and behavioural arms. AAV1-nEF-DIO-eNpHR3.0-p2a-ChR2-YFP (eNPAC) was injected bilaterally into the RSP of Rpb4-cre mice. Illumination was with 20 Hz blue light and constant yellow light, alternating every 250 ms. Results of the hot-plate test after illumination in the RSP and the SS: for RSP, left to right: paw-flick: YFP versus rhythmic, $P = 0.53$; YFP versus random, $P = 0.48$; rhythmic versus random, $P = 0.43$. Paw-lick: YFP versus rhythmic, $^{*}P = 0.034$; YFP versus random, $P = 0.38$; rhythmic versus random, $P = 0.20$. Corrected two-sided unpaired *t*-tests, $n = 8$ YFP, $n = 7$ rhythmic, $n = 7$ random mice. Hedge's *g* effect sizes for flick: −0.31, 0.50, 0.79; lick −1.43, −0.45, 0.80. For SS, left to right: paw-flick: $P = 0.50$; paw-licks: $P = 0.71$; Hedge's *g* effect size for flick: −0.35; lick: −0.19. Two-sided paired *t*-test, $n = 8$ control, $n = 6$ SS eNPAC mice.

Dissociative behaviour tracks RSP rhythm

We next conducted extensive behaviour testing in mice, beginning with reflexive (paw-flick) and affective/self-protective (paw-licking) responses to aversive stimuli (hot-plate test; Fig. 3a). Whereas the administration of ketamine did not reduce reflexive responses (paw-flick, one-way ANOVA, $F_{4,20} = 1.11$, $P = 0.38$)—revealing robustly preserved sensory-detection and motor capabilities—it did abolish affective/emotional (paw-lick, one-way ANOVA, $F_{4,20} = 10.1$, $P < 5 \times 10^{-4}$) and motivational (jump-to-escape, one-way ANOVA, $F_{4,20} = 105$, $P < 1 \times 10^{-12}$) defensive behaviours at doses of 25 and 50 mg kg^{-1} (Fig. 3b, Extended Data Fig. 9a), with similar effects on rearing and behavioural latency (Extended Data Fig. 9b, c).

This separability of stimulus detection from affective response suggested a dissociation-like state. We next explored escape and social interactions on longer timescales. Ketamine at doses of 25 mg kg^{-1} or higher suppressed both tail-suspension escape responses (one-way ANOVA, $F_{4,20} = 9.36$, $P = 0.0002$) and resident–intruder interactions (one-way ANOVA, $F_{4,15} = 13.6$, $P < 0.0001$) to a similar extent (Extended Data Fig. 9d, e); consciousness was maintained as mice ambulated spontaneously and responded to external stimuli. The righting-reflex test for consciousness was preserved in all mice, but was abolished by anaesthetic doses (200 mg kg^{-1}) of ketamine (Extended Data Fig. 9f).

Affective behaviours were consistently preserved after doses of 13 mg kg^{-1} ketamine, yet were selectively abolished at doses of 25 mg kg^{-1}. We therefore directly compared RSP activity between these two doses using fibre photometry with locally expressed GCaMP6m for increased specificity, and widefield imaging for consistency with our earlier data. RSP recordings revealed a 1–3-Hz oscillation after ketamine doses of 25 mg kg^{-1}, but not 13 mg kg^{-1}—suggesting that the 1–3-Hz RSP rhythm could be critical for dissociation-like behavioural effects (Fig. 3c, d).

At dissociative doses, ketamine can also induce analgesia, hallucinations and sedation. We therefore repeated the panel of behavioural experiments with four additional classes of drugs that elicit subsets of these effects. The non-sedative dissociative agent PCP alone recapitulated the ketamine-induced behavioural disconnection between sensory-detection and affective responses in the hot-plate test; like ketamine, PCP also inhibited longer-timescale escape and social behaviours (Fig. 3e, Extended Data Fig. 9g–k), while locomotion velocity was unchanged (Fig. 3f, Extended Data Fig. 9l). Analgesics (centrally acting buprenorphine and topical lidocaine) decreased stimulus-detection foot-flicks; neither diminished escape responses (Extended Data Fig. 9l). The hallucinogen LSD disrupted neither sensory-detection nor affective responses, and tended to increase responsivity to salient stimuli (decreased time-to-jump, increased rearing and socialization) while also reducing locomotion in the stimulus-poor open field. Finally, the sedative diazepam did not recapitulate dissociative-like behaviour.

Together, these results reveal a measurable and consistent dissociation-like behavioural phenotype in mice—characterized by

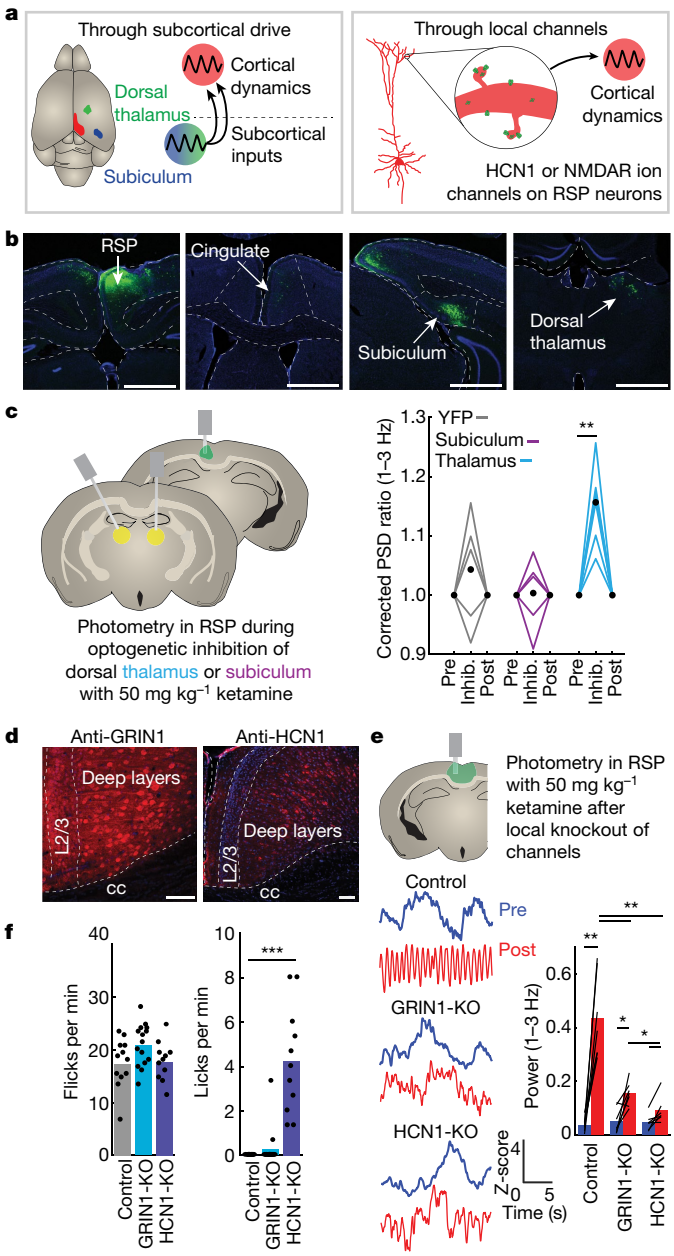

Fig. 4 | RSP HCN1 channels are required for ketamine to induce deep rhythm and dissociation-like behaviour. a, Possible mechanisms underlying RSP rhythm. **b**, Confocal images showing the monosynaptic inputs to the layer 5 RSP, from left to right: RSP, cingulate cortex, subiculum and dorsal thalamus cells. Green, GFP; blue, DAPI. Scale bars, 1 mm. **c**, RSP recording during subcortical inhibition. Left, AAVdj-CaMKIIa-eNpHR3.0-YFP was injected bilaterally into the dorsal thalamus or subiculum, and GCaMP6m was expressed in the RSP. Right, relative power of the 1–3-Hz rhythm before, during and after optogenetic inhibition over 2-min periods beginning 10 min after ketamine injection. Data are normalized by PSD during the pre-period, and then linearly corrected to account for the decrease in oscillation power across the 6-min recording. Thalamus inhibition increased oscillation power (two-sided paired *t*-test, YFP $P = 0.057$, $n = 5$ mice; subiculum $P = 0.91$, $n = 5$ mice; thalamus $P = 0.003$, $n = 7$ mice). Hedge's *g* effect sizes: YFP 0.54; subiculum 0.065; thalamus 2.90. **d**, Confocal microscopy images of immunohistochemistry with antibodies against GRIN1 (left) or HCN1 (right) in wild-type (WT) mice, to reveal channel expression. The HCN1 image reveals low HCN1$^+$ density in the superficial RSP. cc, corpus callosum. Scale bars, 75 µm. **e**, RSP recording after local knockout. Left, photometry experiments in the RSP. AAVs expressing Cre-recombinase and Cre-dependent GCaMP6 were injected to induce local disruption of NMDA-receptor or HCN1-channel expression. Middle, photometry traces of the control, GRIN1 and HCN1 knockout (KO) experiments. Right, reduced ketamine-induced oscillation power was observed in GRIN1- and HCN1-knockout mice. Corrected two-sided paired *t*-test for within-mouse comparison and corrected two-sided independent *t*-test for between genotype comparisons: NS $P > 0.05$, $^*P < 0.05$, $^{**}P < 0.01$, $^{***}P < 0.001$, $n = 7$ mice per group. Hedge's *g* effect sizes: WT-pre/WT-post 3.22; GRIN1-pre/GRIN1-post 2.03; HCN1-pre/HCN1-post 1.02; WT-post/HCN1-post −2.75; WT-post/GRIN1-post −2.26; HCN1-post/GRIN1-post 1.24; WT-pre/HCN1-pre 0.318; WT-pre/GRIN1-pre 0.322; HCN1-pre/GRIN1-pre 0.09. **f**, Results of the hot-plate test on knockout mice after the administration of ketamine. Reflexive paw-flicks (left; corrected Mann–Whitney *U*-test, $P > 0.1$) and affective paw-licks (corrected Mann–Whitney *U*-test, WT versus GRIN1, $P = 0.56$; WT versus HCN1, $^{***}P < 0.001$). Hedge's *g* effect-sizes for flick: 0.77, 0.070; and lick: 0.40, 2.46.

preserved stimulus detection with diminished affective response—that is specifically elicited by dissociative agents at doses corresponding to emergence of the RSP rhythm.

Causal role of RSP layer 5 in behaviour

To test the causal effect of this oscillation, we optogenetically delivered the corresponding activity to RSP layer 5 neurons by co-expressing eNpHR3.0/ChR2 (eNPAC) in layer 5 (Rbp4$^+$) RSP and rhythmically stimulating at 2 Hz (250 ms/20 Hz blue light, alternating with 250 ms continuous yellow light) (Fig. 3g, Extended Data Fig. 10a). Controls included non-opsin-expressing mice, and the non-rhythmic (random) illumination of opsin-expressing mice.

Whereas rhythmic RSP drive did not disrupt reflexive responses, affective paw-licking was reduced compared with control mice (unpaired *t*-test, corrected $P = 0.034$) (Fig. 3g). Rhythmic drive lengthened time-to-escape compared both with mice in which opsin was not expressed (unpaired *t*-test, corrected $P = 0.020$) and with randomly illuminated mice (unpaired *t*-test, corrected $P = 0.054$) (Extended Data Fig. 10b), and rearing was reduced in rhythmically illuminated mice compared with control mice (unpaired *t*-test, corrected $P = 0.020$; Extended Data Fig. 10c, d). Rhythmic illumination significantly diminished tail-suspension escape behaviour (for which repeated within-animal testing was possible) compared with random illumination in eNPAC-expressing mice (paired *t*-test, rhythmic versus random illumination, $P = 0.038$; Extended Data Fig. 10e). Rhythmic drive did not reduce resident–intruder social interactions (paired *t*-test, rhythmic versus random illumination, $P = 0.21$; Extended Data Fig. 10f); righting-reflex and open-field behaviours were unaffected (Extended Data Fig. 10g–k). To test rhythmic optogenetic drive of a different cortical area, we expressed eNPAC in deep layers of the somatosensory cortex; rhythmic illumination in this location did not induce the dissociative behavioural state (Fig. 3g, Extended Data Fig. 10l–o). In summary, in the absence of ketamine, optogenetically providing the activity pattern that naturally arises in layer 5 RSP neurons in response to ketamine exerted the effect of diminishing the connection between sensory and affective responses.

Ketamine effects require RSP pacemaker

We next asked how systemic administration of ketamine could evoke such a layer-specific, focal and behaviourally potent rhythm. We explored two main hypotheses: that long-range subcortical inputs provide a specific oscillatory drive to layer 5 retrosplenial neurons; or that the selective expression of specific ion channels in the RSP facilitates local oscillations (Fig. 4a).

Because thalamic nuclei have been implicated in rhythmicity[23–26] and exhibited oscillations in our electrophysiology experiments, we considered that thalamo-cortical loops might contribute to RSP rhythms. To test this hypothesis, we optogenetically inhibited monosynaptic

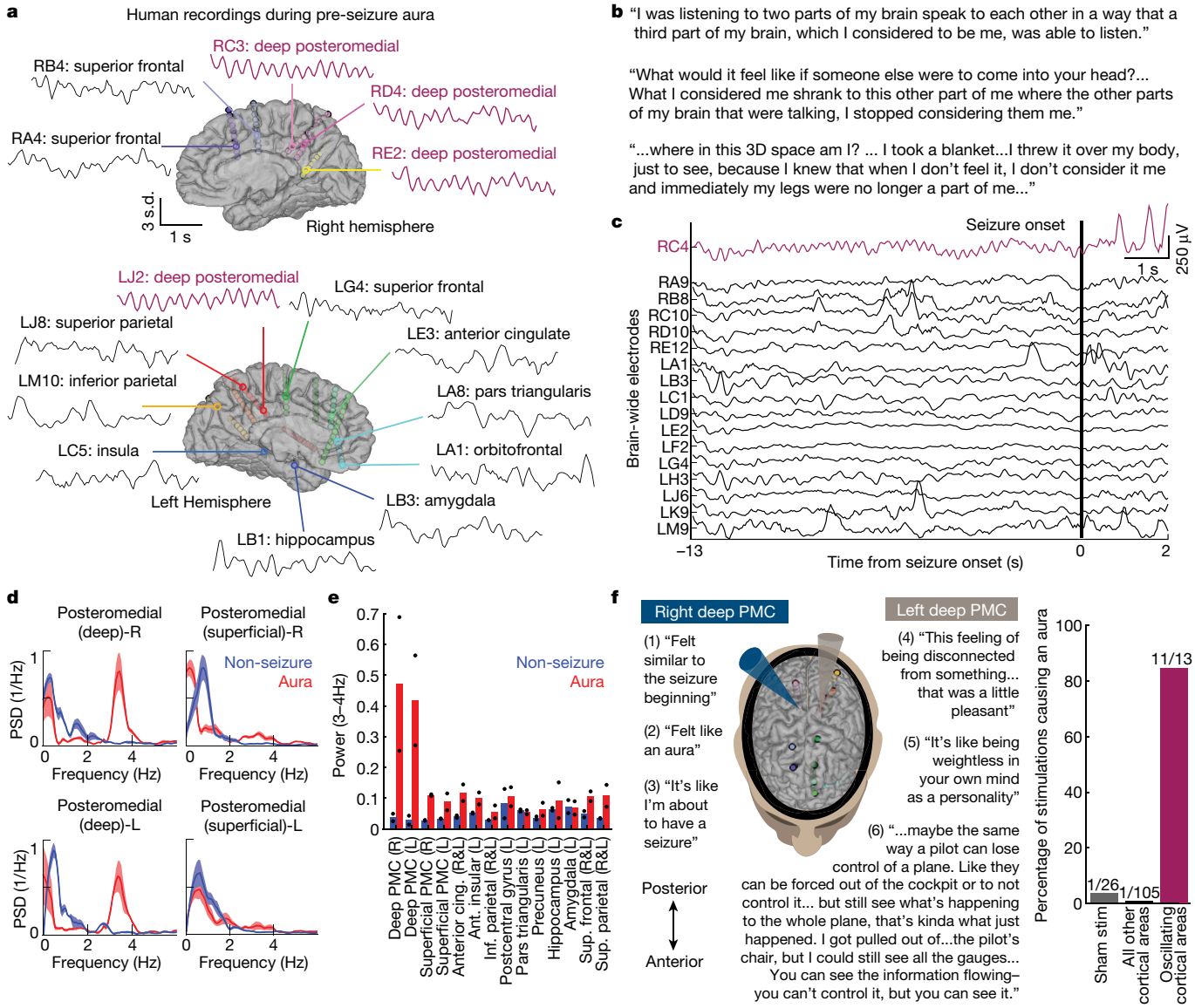

Fig. 5 | Human PMC rhythm and self-reported dissociation. a, Simultaneous iEEG and 3D-electrode locations in a patient, 10 s before seizure onset. Locations are coded as follows (using RC3 as an example): R (right hemisphere) C (electrode letter) 3 (contact number) followed by anatomical region (for example, posteromedial). The rhythm was observed in the PMC in both hemispheres across contacts (magenta) and not in other regions (black). Contacts on each electrode are represented by dots. **b**, Comments from the patient describing their pre-seizure aura experience. Notably, consistently described symptoms of dissociation[13] can involve reproducible perceptions of depersonalization (a feeling of being an outside observer of one's body and/or thoughts) and derealization (feeling of being detached from the surroundings). For the interview transcript, see Supplementary Note 1. **c**, Simultaneously recorded iEEG traces during the pre-seizure period, taken from a different seizure to that shown in **a**. Traces from one contact per electrode are shown in black, and the trace from the deep PMC contact is shown in magenta. Seizure onset was determined by an epileptologist and is marked with a vertical line. **d**, iEEG spectra from the deep and the superficial PMC during aura (red) or non-seizure (blue) periods. Mean ± s.e.m. in right (top) and left (bottom) regions across aura periods. **e**, Power of the 3–4 Hz rhythm during aura (red) or non-seizure/aura period (blue). Mean across channels in each region; the aura periods are shown as a black dot. **f**, Left, locations of electrodes in the brain of the patient (coloured dots). Electrodes in the deep PMC are accentuated with blue (right) and grey (left) indicators. Comments describing the patient's experience during electrical stimulation of the deep PMC are also shown. Right, the percentage of times that aura was reported for each sham or electrical stimulation (≥6 mA).

excitatory inputs (from the dorsal-thalamus or the subiculum) while recording RSP activity after ketamine injection (Fig. 4b, c, Extended Data Fig. 11a, b). Inhibition of the dorsal thalamus did not attenuate, but rather enhanced, the cortical oscillation (paired *t*-test, corrected $P = 0.003$; Fig. 4c, Extended Data Fig. 11c); inhibition of the subiculum (or illumination of control mice) had no effect.

To identify potential rhythm-generators in the RSP, we investigated two candidate channels: NMDA receptors (a primary target of ketamine[27,28] and PCP) and hyperpolarization-activated cyclic-nucleotide-gated potassium channel 1 (HCN1) pacemaker channels (which are involved in spontaneous rhythmic firing[29,30]). Immunohistochemistry of HCN1 channels, but not NMDA receptors, revealed high expression localized in the deep RSP (relative to layer 2/3 RSP and the neighbouring deep visual cortex; Fig. 4d, Extended Data Fig. 11d, i). We recorded from the RSP after NMDAR (GRIN1) or HCN1 channels were genetically disrupted via local injection of AAVdj-Ef1a-Cre and AAVdj-Ef1a-DIO-GCaMP6m viruses into the RSP of adult homozygous floxed-channel transgenic mice, such that GCaMP6m would be expressed only in Cre-expressing and gene-knockout cells (Fig. 4e, Extended Data Fig. 10e, f). After four weeks, ketamine-induced

oscillations were significantly diminished in HCN1 and GRIN1 mice, but preserved in wild-type mice (Fig. 4e, Extended Data Fig. 11g). The use of local-knockout mice enables us to induce a brain state in which all aspects of global ketamine action are preserved except for those that depend on channels in the RSP; furthermore, this can be achieved without directly inhibiting or lesioning the RSP, thus permitting—for example—non-oscillatory RSP activity.

For behavioural experiments, mice were injected in multiple locations across the RSP, yielding a local reduction in protein expression (Extended Data Fig. 11h–j). In control experiments, 50 mg kg^{-1} ketamine abolished affective paw-licking while preserving reflexive paw-flicks—indicative of the dissociative phenotype (Fig. 4f). Injection of the Cre virus into the RSP of HCN1-knockout mice markedly restored affective paw-licking (Mann–Whitney *U*-test, corrected $P < 0.001$); that is, the induction of dissociation-like behaviour by ketamine was blocked. Mice in which both GRIN1 and HCN1 channels were knocked out also showed modest recovery of escape behaviour in the tail-suspension test ($P < 0.001$) and of resident–intruder social interactions ($P < 0.01$) compared with the wild-type, and all mice successfully righted from postural inversion (Extended Data Fig. 11k–n). Without the administration of ketamine, AAVdj-Ef1a-Cre-injected HCN1-knockout and GRIN1-knockout mice exhibited reflexive and affective behaviours comparable to those of wild-type C57BL/6 mice (Extended Data Fig. 10p–s). We therefore conclude that local RSP HCN1 pacemakers are required in order for systemic ketamine to induce the deep RSP rhythm and elicit the dissociation-like behavioural state.

Focal 3-Hz rhythm in human dissociation

A patient at the Stanford Comprehensive Epilepsy Center, who had epilepsy with pre-seizure auras that were described as dissociative, had previously been implanted with brain-wide intracranial electrodes to enable intracranial electroencephalography/stereoelectroencephalography (iEEG) for diagnostic recording and stimulation purposes (Supplementary Note 1). Inspection of the iEEG traces from this patient near the onset of seizures with dissociative aura revealed a prominent rhythmic waveform only in the deep posteromedial cortex (PMC; defined as retrosplenial, posterior cingulate and medio-ventral precuneus cortex; the rodent RSP is considered the closest analogue to human PMC areas[31]) (Fig. 5a–c, Extended Data Figs. 12a, b, 13). Applying the same analyses from the imaging of mice, we discovered a sharp oscillatory profile centred on 3.4 Hz that was restricted to the deep PMC (Fig. 5d, e, Extended Data Fig. 12c). Although the seizure focus was localized to the right hemisphere, the left PMC engaged in simultaneous oscillatory dynamics, giving rise to bilaterality—as was observed in mice.

As part of clinical mapping, brief stimulation (50 Hz, 2–10 mA, total duration 1.3 ± 0.47 s; mean ± s.e.m.) was applied at individual electrodes. To quantify the elicited response from each stimulation in an unbiased fashion, we identified every electrical contact that exhibited rhythmicity during spontaneous dissociative auras (Extended Data Fig. 12d). Stimulation of the seizure focus in the right PMC elicited dissociative, aura-like feelings similar to those at seizure onset (Fig. 5f, comments 1–3). Stimulation of the left PMC elicited immediate and confidently reported dissociative experiences, without the negative valence of an impending seizure (comments 4–6). Stimulations through these spontaneously oscillating PMC contact sites evoked a dissociative aura 11 out of 13 times, whereas almost no non-oscillating contacts responded in this way (Fig. 5f, Extended Data Fig. 12e). Only one sham stimulation elicited report of an aura; this one report followed a real stimulation that had elicited a strong aura. Together, these results demonstrated causal elicitation of human dissociative symptoms local to sites exhibiting the deep PMC rhythm.

Discussion

Here we have used large-scale optical recording technology to enable the discovery of a dissociative-agent-elicited, layer-5-restricted, low-frequency rhythm that is localized to the deep RSP. This rhythm was associated with elicitation of a dissociation-like behavioural state in mice, and precisely paced optogenetic intervention revealed that the rhythmic activity itself was causally linked to the dissociative-like effects. Knockout of HCN1 channels locally in the RSP abolished both the pharmacologically induced rhythm and the dissociation-related behaviour. Conscious experience of human dissociation was linked to endogenous rhythmic activity in the homologous deep PMC. These experiments identified molecular, cellular and physiological properties of a deep posteromedial cortical rhythm that underlies dissociation-like states.

Key aspects of dissociation were recapitulated by three specific interventions: administration of retrosplenial rhythm-inducing doses of ketamine or PCP in mice; rhythmic RSP-localized optogenetic stimulation in mice; and similarly localized electrical stimulation in a patient with epilepsy originating from the right PMC (Extended Data Fig. 14). We note that high-frequency electrical stimulation of the PMC of non-epileptic subjects (spanning superficial and deep regions across many human subjects, in the absence of the epileptic tissue-dependent low-frequency rhythm observed here) does not induce dissociation[32], consistent with our result that low-frequency rhythmic optogenetic drive was specifically and causally linked to dissociative-like behavioural effects. High-frequency electrical intervention—when delivered to epileptic tissue that has specific wiring or ion channel-expression properties—could cause dissociation by several possible cellular mechanisms, including induced rhythmic activity. Likewise, ketamine could induce additional effects in humans or mice—beyond its effects on RSP rhythm—that contribute to its behavioural properties[33–35].

The biophysical mechanisms of both the rhythm and the behavioural state were addressed in mice. HCN1 channels underlie I_h, a hyperpolarization-activated depolarizing current that can pace rhythmic activity; we found that RSP-specific HCN1 disruption selectively abolished both the ketamine-induced rhythm and the dissociation-like behavioural effects. Ketamine blockade of specific depolarizing channels—such as NMDARs—could enable RSP membrane potentials to hyperpolarize, activating intrinsic HCN1 channels and permitting rhythmic dynamics. Our observations regarding the optogenetic inhibition of long-range inputs to the RSP—which enhanced (rather than suppressed) ketamine-induced oscillations—were consistent with this model for HCN1 function in posteromedial cortical rhythmicity, as the long-range inputs are probably glutamatergic and excitatory. Cells with certain high HCN1 expression levels might be most susceptible to this effect—a prediction consistent at the regional level with the spatial pattern of cortical HCN1 expression observed and our TRAP2 activity-localization results. The reliable temporal ordering of the single-unit spike sequence during each oscillation cycle, as observed in our electrophysiology experiments, might reflect the effect of such specific ion-channel expression on membrane dynamics at the single-cell level; future work in humans will be important to further investigate how specific differential expression of rhythm-generating channels might contribute to subjective disorders of dissociation. The effects of GRIN1 knockout were less marked than those of HCN1 knockout, and the magnitude of the rhythm was partially attenuated without recovery of affective behaviour; the remaining oscillatory dynamics could be of sufficient potency to cause dissociation, or alternatively the rhythm-attenuated brain state would be permissive for affective behaviour expression if postsynaptic temporal integration via functional NMDA receptors were intact.

Regarding the functional importance of the ketamine-elicited thalamic oscillation pattern, it is intriguing to consider that the decoupling

of 'primary' thalamic systems (the laterodorsal nucleus (LD) and the anterior ventral nucleus (AV), which are known to connect robustly with posterior forebrain circuitry) and 'secondary' thalamic systems (including the anterior medial nucleus (AM), which projects to the frontal circuitry) could contribute to dissociative symptoms. The inverse correlation of the AM from the AV, LD and RSP could affect autobiographical cognition and egocentricity by disconnecting frontal-cortical areas from posterior-cortical areas, while the 1–4-Hz rhythmicity could maintain continuity of neural activity for periods of more than 200 ms in each subnetwork to preserve conscious mental experience, as distinguished from anaesthesia.

Of all the neocortical regions observed, only the PMC exhibited rhythmic activity that was linked to both dissociative pharmacology and dissociative aura. Notably, previous work had suggested that the effects of NMDAR-antagonizing agents could be greatest in the RSP or in the PMC[36,37], but the capability for independent functional operation of this cortical region—as revealed here—was notable in light of data from many laboratories that point to extensive cortico-cortical wiring and dynamics that integrate the neocortex into a distributed network. Such findings largely originate from task-performing animals, whereas human imaging data report the PMC to be less active in externally oriented tasks and more active during stimulus-independent thought, autobiographical cognition, and mind wandering—all self-oriented, task-independent psychological states[38,39].

Future clinical work could include the exploration of whether electrically induced low-frequency rhythms in the deep PMC of healthy humans can cause dissociative states, and whether dissociative drugs—or dissociation-linked neuropsychiatric states including post-traumatic stress disorder and borderline personality disorder—involve these rhythms in humans. Dissociation in human beings is a self-reported state of mind, and no experimental technique in rodents or in humans can currently define this subjective experience in full. However, the clinically guided paradigm reported here could provide a framework of behavioural, optical and physiological tools to enable exploration of the neural activity that underlies dissociative states. These results highlight the value of new brain-scale recording technologies; here, initial optical and electrical multiregional activity screening guided further quantitative testing of precise causal hypotheses. More generally, integrative technologies with broad and high-resolution perspective could provide increasingly informative experimental access to internal representations of sensations, cognitions and actions at cellular resolution (and with region-wide or even brain-wide perspective), providing a path forward for elucidating the dynamics involved in creating complex brain and behavioural states that are important in health and disease.

Online content

Any methods, additional references, Nature Research reporting summaries, source data, extended data, supplementary information, acknowledgements, peer review information; details of author contributions and competing interests; and statements of data and code availability are available at https://doi.org/10.1038/s41586-020-2731-9.

1. Ferezou, I. et al. Spatiotemporal dynamics of cortical sensorimotor integration in behaving mice. *Neuron* **56**, 907–923 (2007).
2. Mohajerani, M. H. et al. Spontaneous cortical activity alternates between motifs defined by regional axonal projections. *Nat. Neurosci*. **16**, 1426 (2013).
3. Musall, S., Kaufman, M. T., Juavinett, A. L., Gluf, S. & Churchland, A. K. Single-trial neural dynamics are dominated by richly varied movements. *Nat. Neurosci*. **22**, 1677–1686 (2019).
4. Kauvar, I. V. et al. Cortical observation by synchronous multifocal optical sampling reveals widespread population encoding of actions. *Neuron* **107**, 351–367.e19 (2020).
5. Guo, Z. V. et al. Flow of cortical activity underlying a tactile decision in mice. *Neuron* **81**, 179–194 (2014).
6. Wekselblatt, J. B., Flister, E. D., Piscopo, D. M. & Niell, C. M. Large-scale imaging of cortical dynamics during sensory perception and behavior. *J. Neurophysiol*. **115**, 2852–2866 (2016).
7. Ma, Y. et al. Resting-state hemodynamics are spatiotemporally coupled to synchronized and symmetric neural activity in excitatory neurons. *Proc. Natl Acad. Sci. USA* **113**, E8463–E8471 (2016).
8. Allen, W. E. et al. Global representations of goal-directed behavior in distinct cell types of mouse neocortex. *Neuron* **94**, 891–907.e6 (2017).
9. Makino, H. et al. Transformation of cortex-wide emergent properties during motor learning. *Neuron* **94**, 880–890.e8 (2017).
10. Chen, T.-W., Li, N., Daie, K. & Svoboda, K. A map of anticipatory activity in mouse motor cortex. *Neuron* **94**, 866–879.e4 (2017).
11. Xiao, D. et al. Mapping cortical mesoscopic networks of single spiking cortical or sub-cortical neurons. *eLife* **6**, e19976 (2017).
12. Gilad, A., Gallero-Salas, Y., Groos, D. & Helmchen, F. Behavioral strategy determines frontal or posterior location of short-term memory in neocortex. *Neuron* **99**, 814–828.e7 (2018).
13. American Psychiatric Association. *Diagnostic and statistical manual of mental disorders* 5th edn (American Psychiatric Association, 2013).
14. Krystal, J. H. et al. Subanesthetic effects of the noncompetitive NMDA antagonist, ketamine, in humans: psychotomimetic, perceptual, cognitive, and neuroendocrine responses. *Arch. Gen. Psychiatry* **51**, 199–214 (1994).
15. Guo, Z. V. et al. Procedures for behavioral experiments in head-fixed mice. *PLoS ONE* **9**, e88678 (2014).
16. Gil-Sanz, C. et al. Lineage tracing using *Cux2-Cre* and *Cux2-CreERT2* mice. *Neuron* **86**, 1091–1099 (2015).
17. Gerfen, C. R., Paletzki, R. & Heintz, N. GENSAT BAC Cre-recombinase driver lines to study the functional organization of cerebral cortical and basal ganglia circuits. *Neuron* **80**, 1368–1383 (2013).
18. Allen, W. E. et al. Thirst-associated preoptic neurons encode an aversive motivational drive. *Science* **357**, 1149–1155 (2017).
19. DeNardo, L. A. et al. Temporal evolution of cortical ensembles promoting remote memory retrieval. *Nat. Neurosci*. **22**, 460–469 (2019).
20. Oh, S. W. et al. A mesoscale connectome of the mouse brain. *Nature* **508**, 207–214 (2014).
21. Hunnicutt, B. J. et al. A comprehensive thalamocortical projection map at the mesoscopic level. *Nat. Neurosci*. **17**, 1276–1285 (2014).
22. Phillips, J. W. et al. A repeated molecular architecture across thalamic pathways. *Nat. Neurosci*. **22**, 1925–1935 (2019).
23. McCormick, D. A. & Pape, H. C. Properties of a hyperpolarization-activated cation current and its role in rhythmic oscillation in thalamic relay neurones. *J. Physiol. (Lond.)* **431**, 291–318 (1990).
24. Leresche, N., Lightowler, S., Soltesz, I., Jassik-Gerschenfeld, D. & Crunelli, V. Low-frequency oscillatory activities intrinsic to rat and cat thalamocortical cells. *J. Physiol. (Lond.)* **441**, 155–174 (1991).
25. Poulet, J. F. A., Fernandez, L. M. J., Crochet, S. & Petersen, C. C. H. Thalamic control of cortical states. *Nat. Neurosci*. **15**, 370–372 (2012).
26. Fogerson, P. M. & Huguenard, J. R. Tapping the brakes: cellular and synaptic mechanisms that regulate thalamic oscillations. *Neuron* **92**, P687–P704 (2016).
27. MacDonald, J. F., Miljkovic, Z. & Pennefather, P. Use-dependent block of excitatory amino acid currents in cultured neurons by ketamine. *J. Neurophysiol*. **58**, 251–266 (1987).
28. Anis, N. A., Berry, S. C., Burton, N. R. & Lodge, D. The dissociative anaesthetics, ketamine and phencyclidine, selectively reduce excitation of central mammalian neurones by *N*-methyl-aspartate. *Br. J. Pharmacol*. **79**, 565–575 (1983).
29. Ludwig, A., Zong, X., Jeglitsch, M., Hofmann, F. & Biel, M. A family of hyperpolarization-activated mammalian cation channels. *Nature* **393**, 587–591 (1998).
30. Santoro, B. et al. Identification of a gene encoding a hyperpolarization-activated pacemaker channel of brain. *Cell* **93**, P717–P729 (1998).
31. Vogt, B. A. & Paxinos, G. Cytoarchitecture of mouse and rat cingulate cortex with human homologies. *Brain Struct. Funct*. **219**, 185–192 (2014).
32. Foster, B. L. & Parvizi, J. Direct cortical stimulation of human posteromedial cortex. *Neurology* **88**, 685–691 (2017).
33. Moda-Sava, R. N. et al. Sustained rescue of prefrontal circuit dysfunction by antidepressant-induced spine formation. *Science* **364**, eaat8078 (2019).
34. Hua, T. et al. General anesthetics activate a potent central pain-suppression circuit in the amygdala. *Nat. Neurosci*. **23**, 854–868 (2020).
35. Yang, Y. et al. Ketamine blocks bursting in the lateral habenula to rapidly relieve depression. *Nature* **554**, 317–322 (2018).
36. Tomitaka, M., Tomitaka, S., Rajdev, S. & Sharp, F. R. Fluoxetine prevents PCP- and MK801-induced HSP70 expression in injured limbic cortical neurons of rats. *Biol. Psychiatry* **47**, 836–841 (2000).
37. Olney, J. W., Labruyere, J. & Price, M. T. Pathological changes induced in cerebrocortical neurons by phencyclidine and related drugs. *Science* **244**, 1360–1362 (1989).
38. Mason, M. F. et al. Wandering minds: the default network and stimulus-independent thought. *Science* **315**, 393–395 (2007).
39. Raichle, M. E. The brain's default mode network. *Annu. Rev. Neurosci*. **38**, 433–447 (2015).

Publisher's note Springer Nature remains neutral with regard to jurisdictional claims in published maps and institutional affiliations.

© The Author(s), under exclusive licence to Springer Nature Limited 2020

Methods

Experimental model and subject details

All procedures were performed in accordance with protocols approved by the Stanford University Institutional Animal Care and Use Committee (IACUC) and guidelines of the National Institutes of Health. Mouse strains used were *C57BL/6J* (Black 6, Jackson Laboratory (JAX), 664), *Tg(Thy1-GCaMP6s)GP4.3Dkim* (Thy1-GCaMP6s, JAX, 024275), *Cux2-CreERT2* (gift from S. Franco, University of Colorado), *Ai148(TIT2L-GC6f-ICL-tTA2)-D* (Ai148, JAX, 030328) (gift from H. Zeng, Allen Institute for Brain Science), *Tg(Rbp4-cre)KL100Gsat* (Rbp4-Cre, No. 031125-UCD, MMRRC) (L. Luo), *B6.129S-Hcn1tm1Kndl/J* ($HCN1^{f/f}$ JAX, 028299) (gift from L. Giocomo, Stanford University), *B6.129S4-Grin1tm2Stl/J* ($NR1^{f/f}$ JAX, 005246). Male and female mice were used, aged 6–24 weeks at the time of surgery. Mice were group-housed in plastic cages with disposable bedding on a standard 12 h light cycle until surgery and behavioural studies, when they were moved to a 12 h reversed light cycle.

Drug administration

Drugs used were ketamine (VEDCO, ketamine HCl, 6–200 mg kg^{-1}), phencyclidine (PCP, 5 mg kg^{-1}, Sigma-Aldrich P3029), memantine (50 mg kg^{-1}), MK801 (0.75–1 mg kg^{-1}), dexmedetomidine (0.35–1.5 mg kg^{-1}), propofol (35–140 mg kg^{-1}), xylazine (AnaSed AKORN, 12.5 mg kg^{-1}), buprenorphine SR (2 mg kg^{-1}), lidocaine (topical), LSD ((+)-lysergic acid diethylamide (+)-tartrate (2:1), 0.3 mg kg^{-1}) and diazepam (2 mg kg^{-1}). For all imaging, recording and behavioural experiments, drugs were injected intraperitoneally (i.p.) (with a 26-gauge needle) 10 min before data was taken unless noted otherwise (for example, see ketamine injection for Neuropixels experiment in section 'Simultaneous recording from four Neuropixels probes with i.p. drug delivery'). For injection during imaging or Neuropixels recording, a catheter was implanted intraperitoneally before head-fixation (BD Saf-T-Intima, 383323). For anti-depressant effects, human doses are typically 0.3–1 mg kg^{-1}, and in mouse 3–10 mg kg^{-1}. Following the same pattern, humans consistently report potent dissociation at doses of around 2–3 mg kg^{-1}, and in the mouse, the lowest tested dose causing the oscillation and behavioural effects was 25 mg kg^{-1} (refs. [40–42]). Thus, the dose–response relationship for the dissociative effects of ketamine in mice corresponds with human/mouse mapping for previously studied effects of ketamine. Note that the oscillation induced by ketamine is not likely to be a seizure (Supplementary Note 2).

Pan-cortical imaging with blood autofluorescence correction

As described[8], mice were anaesthetized with isoflurane, the scalp was removed, the skull cleaned and dried, and a custom head-plate was cemented to contacts over the cerebellum and in front of the olfactory bulb. The skull was then covered in a thin layer of cyanoacrylate glue (Apollo 2000, Cyberbond), clear dental acrylic (Ortho-Jet, Lang Dental), and clear nail polish (Electron Microscopy Services). Buprenorphine SR (0.1 mg kg^{-1}) was injected subcutaneously for pain management. Mice were given at least one week to recover before experiments. Imaging was performed on a custom-built fluorescence microscope designed for high light collection efficiency and large field of view. The microscope consisted of back-to-back 50 mm f/1.2 camera lenses (Nikon), separated by a FF495-Di03-50.8-D dichroic mirror (Semrock), mounted in a 60 mm cube (Thorlabs). An F-mounted ORCA Flash 4.0 (Hamamatsu) was used to record images, with a FF01-520/35-50.8-D emission filter (Semrock). Alternating 410 nm and 488 nm illumination for non-Ca^{2+} dependent artefact removal was controlled using a microcontroller (Arduino) slaved to the frame output trigger of the camera.

Two-photon imaging

Mice were anaesthetized with isoflurane and the skull above the RSP was removed and replaced with a 7 mm circular glass coverslip. For layer 1 experiments, Thy1GCaMP6s mice were used. For layer 2/3 experiments, Cux2-CreER;Ai148 mice were used (4-hydroxytamoxifen (4-OHT) dissolved in corn oil was injected intraperitoneally at 0.1 mg g^{-1} at least 2 weeks before imaging). For layer 5 experiments, Rbp4-Cre mice were injected locally in the RSP with 800 nl AAVdj-Ef1a-DIO-GCaMP6f (titre 5E12) at stereotactic coordinates −3AP, 0.5ML, −0.6DV (AP, anterior–posterior; ML, medial–lateral; DV, dorsal–ventral). Mice were given at least 1 week to recover before imaging. Awake, head-fixed imaging was performed on a standard two-photon microscope (NeuroLabWare). A 16× 0.8 NA Nikon objective was immersed in clear ultrasound gel for imaging (Aquasonic, Parker Laboratories); frame rate of 30 Hz. Although we observed oscillations in the RSP with a 50 mg kg^{-1} dose of ketamine, we were concerned that 50 mg kg^{-1} may be too low a dose to sensitively detect a potentially weaker signal in the visual cortex or layer 2/3, and so we used a dose of 80 mg kg^{-1} in these experiments.

Ketamine-TRAP experiments

Dissolved 4-OHT (20 mg ml^{-1} in ethanol) was mixed with corn oil at a concentration of 10 mg ml^{-1}, and ethanol evaporated by vacuum centrifugation (60 min). Mice were each placed alone in a novel cage for 30 min, in which they remained for the duration of the experiment. Two mice were injected with 50 mg kg^{-1} ketamine intraperitoneally, and two mice were injected with an equivalent volume of saline. After 1 h, all mice were injected with 50 mg kg^{-1} 4-OHT, as well as an additional dose of 50 mg kg^{-1} ketamine or saline. After 1 h, a final dose of ketamine or saline was administered. This protocol was designed to ensure that the ketamine-induced oscillation (and associated cFos expression) was occurring throughout the majority of the approximately 4 h post-tamoxifen-injection time window during which TRAP2 labels cells. After 10 days (to allow time for expression of tdTomato), mice were perfused with ice-cold PBS and 4% PFA. Coronal sections (50 µm) were taken using a vibratome and imaged on an epifluorescence microscope.

Retrosplenial targeted recordings

Mice were anaesthetized with isoflurane, a small craniotomy (around 2 mm in diameter) was performed above the RSP, and a custom head-plate implanted. The dura was gently removed, and then covered with Kwik-Cast Sealant (World Precision Instruments). A skull screw was implanted and secured with cement in the right frontal skull bone. Mice were given 1–2 h to recover. Next, mice were i.p. injected with 50 mg kg^{-1} ketamine, and head-fixed under an in vivo electrophysiology recording apparatus. To record neural activity, a 32-channel two-shank silicon neural probe (ASSY-37 P-1, Cambridge NeuroTech) was slowly lowered into the RSP. The deepest tip of the electrode was 800–1,000 µm from the brain surface for all recordings.

Simultaneous recording from four Neuropixels probes with i.p. drug delivery

Surgeries. Mice were anaesthetized with isoflurane, carefully levelled in a stereotaxic apparatus and their scalp and periosteum were removed. A 3% hydrogen peroxide in saline solution was used to clean the surface of the skull. A custom stainless steel headbar was levelled on the skull and attached using clear dental cement. After the cement had dried, targeted probe entry sites were stereotaxically marked on the cement layer with a permanent marker (Day 1: 'mPFC', 2.3AP, 0.6ML; 'somatosensory', −0.7AP, −4.0ML; 'retrosplenial', −2AP, −1ML; 'subiculum', −3.5AP, 2.14ML; Day 2: 'OFC': 2.5AP, 1.5ML; 'mPFC': 2.3AP, −0.6ML; 'retrosplenial', −2AP, 1ML; 'thalamus', −1.5AP, −1.7ML). In part, they were selected to cover areas with known connectivity to the RSP. A 2-mm-long insulated platinum–iridium wire was implanted centrally over the cerebellum, with the last several hundred micrometres bared to serve as an electrical reference. Buprenorphine SR was administered to relieve pain and mice were allowed to recover for at least one week before recordings began.

Electrophysiological recording. Mice were acclimatized to head fixation and the recording rig for several days before recording. Several hours before recording, mice were anaesthetized for approximately 30 min each while small 1-mm craniotomies were made over four pre-marked areas. Craniotomies were kept clean of bone fragments and made such that bleeding was minimized. The skull was covered with a pool of saline and with Quik-Cast to protect and keep craniotomies moist before recording. Mice recovered in their home cages before recording. Immediately before recording set up, mice were very briefly anaesthetized with isoflurane and implanted with an intravenous catheter system (BD Saf-T-Intima Closed IV Catheter System: 22G × ¾″, containing an integrated Y adaptor and safety lock) to their intraperitoneal cavity and affixed with glue. The microtubing had been previously loaded with a ketamine in saline solution (0.1 ml of 100 mg ml^{-1} ketamine solution (KetaVed, VEDCO) in 2 ml of saline) and was maintained at neutral pressure using a syringe attached at the distal (from the mouse) end of the fluid line. While still anaesthetized, mice were head-fixed and tubing was secured stably to a custom mouse holder by tape. Quik-Cast was removed from the skull, and craniotomies were briefly cleaned before being submerged in a pool of saline. Four Neuropixels 1.0 probes[43,44], were grounded together with the mouse reference electrode, coated with red fixable dye (CM-DiI, Thermo Fisher), positioned over each craniotomy, and carefully inserted at approximately 15 degrees from the vertical axis to depths of 4–5 mm at a rate of approximately 3 μm s^{-1}. After the completion of all insertions, the probes were allowed to rest for at least 10 min before the recording began. 30 kHz data was acquired from the four probes simultaneously using the Neuropixels control system (as described in the User Manual) and SpikeGLX software (http://billkarsh.github.io/SpikeGLX/). The four acquisitions were synchronized using a common squarewave signal recorded for all probes and aligned to the nearest pulse edge. Following the beginning of recording, a 20 min baseline period of activity was collected. A 50 mg kg^{-1} dose of ketamine was then remotely injected i.p. through the catheter system, the administration time was marked, and an additional 40 min of activity were recorded. After recording, craniotomies were sealed and the skull was covered with Kwik-Cast. A custom MATLAB script wrapping Kilosort2[45] (https://github.com/MouseLand/Kilosort2) functions was used to spike sort data, using default Kilosort2 parameters. After spike sorting with Kilosort2, clusters were manually curated in Phy (https://github.com/cortex-lab/phy) to separate 'Noise' clusters from 'Good' clusters. Clusters were considered 'Noise' if they contained electrical artefacts, were not well isolated, or seemed to drift off of the probe (trend in decreasing amplitude correlated with decreasing spike rate). Subsequent analysis was performed using custom Python code.

Histology. Mice were perfused with phosphate buffered saline (PBS) and 4% paraformaldehyde (PFA) before overnight post-fixation in 4% PFA at 4 °C. Post-fixed brains were maintained for less than 1 week at 4 °C in PBS until subsequent use. Brains were dehydrated in a methanol gradient and subsequently processed as described previously[46]. Whole brains were imaged with horizontal optical sections on a LaVision light sheet microscope in dibenzyl ether for 488 nm autofluorescence and 532 nm CM-DiI electrode tracts. Image stacks were downsampled to 25 μm resolution and registered using autofluorescence signal to the Allen Brain Atlas CCFv3. Nonlinear registration and transformation was performed using Elastix. Transformed CM-DiI electrode tract data was traced in CCF coordinates using a custom variant of AllenCCF software (https://github.com/cortex-lab/allenCCF) and subsequently processed using custom Python code for tract reconstruction and location assignment. Well-isolated unit locations were assigned to the electrode location with peak unit amplitude. This location was used to label a unit with the nearest reference atlas subdivision. Reconstructed tracts were manually assigned to corresponding Neuropixels probe recordings. As individual probe insertions were distant from each other and labelled by hemisphere on the day of insertion, 8 tracts per brain (from two sessions of recording per mouse) could be unambiguously assigned.

Data analysis. After recording time synchronization for all spike times (as described above in the section 'Electrophysiological recording'), spikes for each 'Good' unit were binned at 10-ms intervals and smoothed using a 50-ms width causal moving average filter, resulting in a smoothed spike rate. When shown, spiking data are not binned or smoothed. Correlations were computed using smoothed spike rate traces. For correlations with the RSP, a single trace was computed with the RSP as the mean firing rate across all units in the RSP. This RSP trace was then correlated separately with the firing rate of each individual unit from that recording session. Firing rate was computed as the mean smoothed spike rate across the designated four minute window before or after ketamine administration (either minutes −12 to −8 or +8 to +12). For plotting *z*-scored traces, for each trace, its mean was subtracted and it was divided by its standard deviation. To select units for showing in raster plot, units were sorted on the basis of their correlation of their smoothed spike rate with the mean smoothed spike rate across all RSP units, and the top five units from each region were shown.

Fibre photometry

A 405 nm and 470 nm LED illumination (Thorlabs) was combined (425 nm longpass, Thorlabs DMLP425) and coupled into a fibre-optic patch cord (400 μm diameter, 0.48 NA, Doric Lenses) using a longpass dichroic (505 nm, Thorlabs DMLP505) and a fixed-focused coupler/collimator with a standard FC connector (F240FC-A, NA 0.51, f = 7.9mm)[47,48]. Each illumination channel was frequency-modulated using the sync output from a lock-in amplifier (SR810 DSP, Stanford Research Systems). GCaMP fluorescence was collected through the same patch cord and delivered through a bandpass emission filter (Semrock, FF01-520/35) onto a NewFocus 2151 femtowatt silicon photoreceiver (Newport, DC Low mode). The signal from the photoreceiver was split into each lock-in amplifier, and the filtered outputs were digitized at 5 kHz using a NIDAQ (National Instruments PCIe-6353) and saved using a MATLAB (MathWorks) acquisition script.

General statistical analysis

Sample sizes were chosen using standards in the field established in previous published studies and our laboratory's experience with the behavioural tests. Mean ± s.e.m. was used to report statistics unless otherwise indicated. The statistical test used and the definition n for each analysis is listed in the text or figure legends. Multiple comparisons were false-discovery-rate (FDR)-corrected by Benjamini–Hochberg correction (α = 0.05) and are indicated in the text as 'corrected P'. No statistical methods were used to pre-determine sample size. Criteria for animal exclusion was pre-established: mice were excluded if the injected virus did not express or if optical fibres were mistargeted. Variances were similar between groups that were statistically compared except in a few cases in which the mean and variance were near zero. Effect size was calculated using either Hedge's g, or Glass's Δ was used if group variances were very different.

Widefield imaging and fibre photometry

Analysis was performed using custom MATLAB (MathWorks) scripts. Widefield imaging videos were registered to a 2D top-projection atlas generated from the annotated Allen Brain Atlas volume, version CCFv2, in MATLAB (MathWorks), using an affine transformation computed from four manually selected control points. Each video was dF/F normalized, using the median fluorescence intensity for each pixel over the entire time series as F. The 410 nm channel was then temporally smoothed using a moving average (width = 400 ms). The smoothed 410 nm dF/F signal for each pixel was regressed onto the 488 nm dF/F signal for the corresponding pixel, and the regression coefficients

were used to scale the 410 nm channel to the 488 nm channel. This scaled 410-nm dF/F signal was then subtracted from the 488 nm dF/F signal to produce a normalized signal for each pixel. For quantification, activity traces were extracted from points centred in five cortical regions (visual, somatosensory, parietal, motor, retrosplenial) on the left hemisphere of the brain. The video data was Gaussian smoothed spatially (radius = 2 pixels). Similarly, for fibre photometry recordings, the 410 nm signal was regressed onto the 488 nm signal, the 410 nm signal was scaled by the regression coefficients, and then subtracted from the 488 nm signal.

Two-photon imaging

Two-photon tiff stack videos were registered to the average image using the TurboReg ImageJ plug-in using rigid body transformations. Cellular region of interests (ROIs) were manually selected, because automated algorithms did not perform well in detecting cells with oscillatory activity. Contaminating neuropil signal was estimated from an annulus surrounding each soma mask and removed using the function $F(t) = F\text{soma}(t) - 0.3 \times F\text{neuropil}(t)$, where Fsoma(t) is the somatic dF/F and neuropil(t) is the dF/F from an annulus 4 pixels wide surrounding each soma mask. The resulting traces were detrended and z-scored. The full frame fluorescence (used for quantifying layer 1 neuropil oscillations) was computed by summing all of the pixels in each frame on each time point, and then computing dF/F the same way, with no neuropil subtraction step.

Frequency analysis

Each trace (corresponding to either a fibre photometry signal, a cellular two-photon signal, a widefield regional centroid, a widefield pixel, an iEEG trace or a smoothed spike rate Neuropixels trace) was z-scored, and the PSD was then estimated using Welch's method (pwelch() in MATLAB), with a window size of 10 × fs (15 × fs for human iEEG) where fs is the sampling rate of the signal. The average band power within a specified band (that is, 1–3 Hz) was then computed by integrating the PSD estimate (bandpower() in MATLAB). For displaying the traces of individual cells, traces were each z-scored by subtracting the mean value of the trace (across the whole recorded time window) and dividing by the standard deviation of the trace. Unless otherwise indicated, the PSD was computed across the time window from minutes 10 to 11 post-injection.

32-channel acute silicon probe recordings

Extracellular electrophysiological data were recorded using 32-channel acute silicon probes (ASSY-37 P-1, Cambridge Neurotech) acquired at 30 kHz. Following common average referencing, well-isolated single units were identified using KiloSort and Phy. Data were analysed using custom MATLAB scripts. Instantaneous firing rate was computed using 1 ms bins. We used a hidden Markov model with two states to label ON and OFF states. ON states were considered to represent bursts, and OFF states were inter-burst intervals. We fit the emission and transition parameters of the model using the Baum–Welch algorithm (MATLAB hmmtrain with a convergence threshold of 1×10^{-6} and initial guesses of transition matrix: [0.95, 0.05; 0.05, 0.95] and emission: [0.5, 0.5; 0.1, 0.99]), and then estimated the state assignment at each time point using the Viterbi algorithm (MATLAB hmmviterbi). Various initial guesses were tested, and they yielded the same or similar model fit. For population analyses, a bin size of 2 was used. In Extended Data Fig. 5, we look at the number of spikes in each burst, which can vary depending on the neuron being recorded, so we included every burst for every neuron. To quantify the consistency of the sequential onset of activation across bursts, we ranked each unit by its onset time for each burst. We then ordered the units according to their median rank across bursts. For each burst, we fit a linear model between the ranking in that burst and the median rank. The distribution of correlation coefficients was then plotted across bursts for each mouse and treatment condition.

Rodent behaviour

General behavioural notes. Mice were handled and acclimatized to patch cord coupling before testing. Opsin and control mice were randomly distributed across group-housed experiment cages. Experimenters were blinded to the identity of the mice during performance and scoring of each behavioural assay, as well as when assessing viral expression and fibre placement. For all statistical tests between groups and involving multiple comparisons, a Benjamini–Hochberg FDR correction was used.

Hot-plate test. Mice were placed on the hot plate (Bioseb), which was set to 55 °C and surrounded by a clear circular perimeter. Mouse activity was recorded using two cameras from different angles. The experiment ended when the mouse jumped to escape or when 90 s had elapsed. Care was taken to clean and dry the hot plate apparatus between mice. For optogenetic experiments, mice were connected to patch cords and then returned to a holding cage. Illumination began 30 s before mice were placed on the hot plate.

Tail suspension test. Mouse activity was recorded using a 60-Hz web camera. Struggling activity was quantified for minutes 2–10. For ketamine experiments, tail suspension began 5 min after injection, so that post-injection minutes 7–15 were used for scoring. For optogenetic experiments, mice were connected to patch cords and then returned to a holding cage. Illumination began 30 s before tails were secured with tape and suspended from the beam. Mice were excluded if they climbed on their own tails.

Social interaction assay. Resident–intruder social interaction was recorded for two minutes. Interactions were defined as close physical proximity behaviours, including sniffing, touching and following. For optogenetic experiments, mice were connected to patch cords and then returned to their home cage. Illumination began 30 s before the same-sex intruder mouse was introduced.

Righting reflex assay. Mice were held at the neck and tail, rotated to supine position on a flat surface, and quickly released. Time to right was quantified as moment of release to moment when all 4 legs touched the ground. A five second threshold was used to classify righting success (less than 5 s) from failure (more than 5 s). For optogenetic experiments, mice were connected to patch cords and then returned to a holding cage. Illumination began for 30 s, and then the mouse was swiftly inverted onto the flat surface.

Open field test. Mice were placed in an evenly illuminated 50 cm × 50 cm open field test box. Mouse position was captured using a webcam and Viewer software (Biobserve).

Retrosplenial optogenetics

Stereotaxic surgery. Adult male and female Rbp4-Cre transgenic mice were bilaterally injected with either 1 µl of AAV1-nEF-DIO-eNpHR3.0-p2a-ChR2(H134R)-YFP (titre 5E12, known as eNPAC 2.0, and referred to in the text as eNPAC) or AAV5-Ef1a-DIO-eYFP (titre 5E12) in the RSP (AP −3.3, ML ± 0.5, DV 0.5). A fibre was implanted above each injected area. For S1 opsin-expressing mice, the injection was made at AP +0, ML ± 3.0, DV 0.5. Viruses were obtained from the Stanford Neuroscience Gene Vector and Virus Core. Mice were given four weeks for viral expression and recovery before experimentation.

Illumination parameters. For blue light: 473-nm laser, 10-ms pulses, 20 Hz, 20 mW at fibre tip. For yellow light: 594 nm, continuous light, 15 mW at fibre tip. Alternating 250-ms bouts of pulsed blue light and continuous yellow light were used for oscillatory stimulation experiments. For non-rhythmic stimulation, alternating 20 Hz blue light and

continuous yellow light were also used but with the length of each illumination randomly selected from a uniform distribution with a minimum of 50 ms and a maximum of 2 s. Each 30 s, blue light and yellow light pulse length was selected such that the total time allotted to blue or yellow light across 30 s matched that of the rhythmic group.

Subcortical projection optogenetics with fibre photometry

Stereotaxic surgery. Adult male and female wild-type C57/BL6 wild-type mice were bilaterally injected into the dorsal anterior thalamus (AP −1.2, ML ± 1, DV 3.25) or subiculum (AP −3.8, ML ± 2.5, DV −2.2) with 500 nl of either AAVdj-CaMKIIa-NpHR3.0 (titre 5.15E12) or AAV8-Ef1a-eYFP (titre 5E12). Then, 500 or 600 nl of AAVdj-CaMKIIa-GCaMP6m was injected into the right RSP (AP −3.3, ML 0.5, DV 0.5). A fibre was implanted above each injected area (with one of the subcortical fibres angled at 30°). Four weeks were allowed for viral expression and recovery before experimentation.

Illumination parameters. Illumination was performed with 594 nm, continuous light, with a power of 15 mW at each fibre tip. Eight minutes after the administration of ketamine (50 mg kg^{-1}), six minutes of photometry data were recorded: two minutes of pre-illumination photometry were recorded, followed by two minutes with continuous illumination, and then two minutes of post-illumination.

Histology. For monosynaptic input tracing, adult male Rpb4-cre mice were injected with AAV8-EF1a-DIO-TVA-p2A-oG (9E12) into the RSP. Two weeks later, ENVA-Rabies-GFP (3E8) was injected in the same location. After five days, mice were perfused, brains fixed overnight, and sectioned into 50-µm sections; full coronal sections were imaged on a confocal microscope for cell counting.

Retrosplenial gene disruption and fibre photometry

Stereotaxic surgery. Adult male and female $HCN1^{f/f}$, $NR1^{f/f}$, or wild-type C57/BL6 mice were injected bilaterally in two retrosplenial locations (AP −3.1 and −3.4, ML ± 0.5, DV −0.5) with 1 µl of AAV8-Ef1a-mCherry-IRES-Cre (titre 5E11) and AAVdj-Ef1a-DIO-GCaMP6m (titre 1E13). A 400-µm optical fibre was implanted over one injection location. At least four weeks were allowed for viral expression and gene disruption before photometry recording. For gene knockout behaviour experiments, injections of AAVdj-Ef1a-Cre were made at AP −2.7, −3.1 and −3.5; ML ± 0.5; DV −1.35 and −0.70. For gene knockout control behavioural experiments, two retrosplenial injections of AAVdj-Ef1a-Cre were made in experimental mice.

Rodent histology. After PFA-perfusion and overnight fixation in 4% PFA at 4C, 50 µm sections were taken on a vibratome. For immunohistochemistry, sections were washed in PBST (0.3% Triton-X) for 1 h, blocked with 1% BSA for 30 min, and then incubated with primary antibody in 1%PBST-BSA overnight. Primary antibodies used were anti-HCN1: 1:500 of abnova MAB6651 lot MH387188, anti-NMDAR: 1:500 of Invitrogen RA5-85751, lot UF2785857C. Next, sections were washed for 30 min in 1% PBST and then incubated with secondary antibody (1:500 in PBST-BSA) for 90 min at room temperature, and then washed for 1 h in PBST. Sections were mounted on slides and imaged using a confocal microscope.

Human iEEG recordings

All clinical research was reviewed and approved by the Stanford Institutional Review Board. Informed consent was obtained from the subject before participation in the study protocol. The patient (participant number S19-137/SD056) was implanted with Ad-Tech iEEG Depth Electrodes as part of routine phase II monitoring for refractory epilepsy. A 10 kHz research copy of the patient's electrophysiological data was acquired over Ethernet, simultaneous with inpatient clinical recording, via a Nihon Khoden JE-120A junction box as part of an EEG-1200 clinical acquisition system, stored using EEGStorage v.1.13, and processed via Python. For ease of processing, the 10-kHz data were decimated to 20 Hz using a 20th-order FIR filter to evaluate the 3-Hz features. Key times surrounding seizures were reviewed at 10 kHz. Video of the patient, aligned to the electrophysiology with about 100-ms precision, was part of the clinical record and was reviewed to acquire patient quotes during stimulation mapping. For quantification, 10 s of pre-seizure data were used, *z*-scored, and the PSD was then estimated using Welch's method (pwelch() in MATLAB). The average band power within a specified band (3–4 Hz) was then computed by integrating the PSD estimate (bandpower() in MATLAB). There was still an increase in band power in the PMC during pre-seizure auras relative to non-seizure periods and to other regions when using the 1–4-Hz band, but there was baseline low- frequency power in all regions that made the effect of the approximately 3-Hz oscillation smaller. The clinical stimulus pulse pattern used was the standard protocol of 50-Hz biphasic stimulation for 1–2 s, and no other stimulation frequencies were attempted.

Reporting summary

Further information on research design is available in the Nature Research Reporting Summary linked to this paper.

Data availability

The datasets generated and analysed are available from the corresponding author upon reasonable request and at https://www.optogenetics.org. Source data are provided with this paper.

Code availability

Code used for data processing and analysis is available from the corresponding author upon reasonable request.

40. Kohrs, R. & Durieux, M. E. Ketamine: teaching an old drug new tricks. *Anesth. Analg.* **87**, 1186–1193 (1998).
41. Green, S. M., Roback, M. G., Kennedy, R. M. & Krauss, B. Clinical practice guideline for emergency department ketamine dissociative sedation: 2011 update. *Ann. Emerg. Med.* **57**, 449–461 (2011).
42. Schwenk, E. S. et al. Consensus guidelines on the use of intravenous ketamine infusions for acute pain management from the American Society of Regional Anesthesia and Pain Medicine, the American Academy of Pain Medicine, and the American Society of Anesthesiologists. *Reg. Anesth. Pain Med.* **43**, 456–466 (2018).
43. Jun, J. J. et al. Fully integrated silicon probes for high-density recording of neural activity. *Nature* **551**, 232–236 (2017).
44. Putzeys, J. et al. Neuropixels data-acquisition system: a scalable platform for parallel recording of 10 000+ electrophysiological signals. *IEEE Trans. Biomed. Circuits Syst.* **13**, 1635–1644 (2019).
45. Stringer, C. et al. Spontaneous behaviors drive multidimensional, brainwide activity. *Science* **364**, eaav7893 (2019).
46. Allen, W. E. et al. Thirst regulates motivated behavior through modulation of brainwide neural population dynamics. *Science* **364**, eaav3932 (2019).
47. Zalocusky, K. A. et al. Nucleus accumbens D2R cells signal prior outcomes and control risky decision-making. *Nature* **531**, 642–646 (2016).
48. Gunaydin, L. A. et al. Natural neural projection dynamics underlying social behavior. *Cell* **157**, 1535–1551 (2014).
49. Lein, E. S. et al. Genome-wide atlas of gene expression in the adult mouse brain. *Nature* **445**, 168–176 (2007).

Acknowledgements This work was supported by grants to K.D. from the National Institute on Drug Abuse (NIDA P50 Center), NIMH, DARPA, the Tarlton Foundation, the AE Foundation Borderline Research Fund, the NOMIS Foundation and the Else Kroner Fresenius Foundation. K.D. and L.L. were additionally supported by the NSF NeuroNex program. S.V., I.V.K. and E.R. are supported by a National Science Foundation Graduate Research Fellowship. F.G. is supported by a Walter V. and Idun Berry Postdoctoral Fellowship, a NARSAD Young Investigator Award, and a K99/R00 award from NIDA. J.H. and P.N. are supported by a Stanford Bio-X Interdisciplinary Initiatives Seeds Grants Program. P.N. received funding from the Wu Tsai Neurosciences Institute. J.P. is supported by R01MH109954 from the National Institutes of Mental Health. We thank J. H. Lui (Rbp4-Cre), S. Franco (Cux2-CreER), K. Masuda and L. Giocomo (HCN1), and W. E. Allen for contributing to widefield imaging and Neuropixels systems; C. Ramakrishnan for virus assistance; and S. Pak, A. Chibukhchyan, N. Pichamoorthy, C. Lee and C. Delacruz for administrative support and animal husbandry. We acknowledge L. Williams and L. Tozzi for detailed discussions regarding human imaging; and L. Giocomo, B. Heifets, B. Knutson, L. Fenno, E. Sylwestrak, Y. Chen, X. Sun, T. Machado and J. Kochalka for discussion. We thank members of the Stanford Comprehensive Epilepsy Center, including H. Kaur, T. Pham, L. Schumacher, D. Sebrell, A. Valderde, A. Joshi, M. Market, C. Halpern and

B. Razavi. We also thank the Clinical Imaging and Stimulation subgroup in our laboratory for discussion and collaboration.

Author contributions S.V., I.V.K. and K.D. designed experiments and wrote the paper. S.V. and I.V.K. collaborated closely to perform all mouse experiments, analyse all datasets and make all figures. E.R. constructed the Neuropixels rig, designed Neuropixels experiments, performed recordings and processed data under the guidance of K.D. and L.L. S.V., I.V.K. and E.R. analysed Neuropixels data and made figures. F.G. performed electrophysiological recordings, analysis and made figures under the guidance of K.D. and R.C.M. J.M.H. performed the implantation of the epilepsy monitoring electrodes in the human research patient. J.P., J.M.H., P.N., T.O. and C.S.-S. collected human iEEG data. T.O. and P.N. performed human iEEG data curation and processing. J.P. performed the human electrical stimulation procedure. All authors made comments on the manuscript. K.D. supervised all aspects of the work.

Competing interests All tools and protocols used during this study are freely available for non-profit use from the corresponding author upon request. Stanford University is in the process of submitting a patent application to further facilitate therapeutic translation of the findings reported in this study.

Additional information

Supplementary information is available for this paper at https://doi.org/10.1038/s41586-020-2731-9.

Correspondence and requests for materials should be addressed to K.D.

Peer review information *Nature* thanks Thomas J. McHugh and the other, anonymous, reviewer(s) for their contribution to the peer review of this work.

Reprints and permissions information is available at http://www.nature.com/reprints.

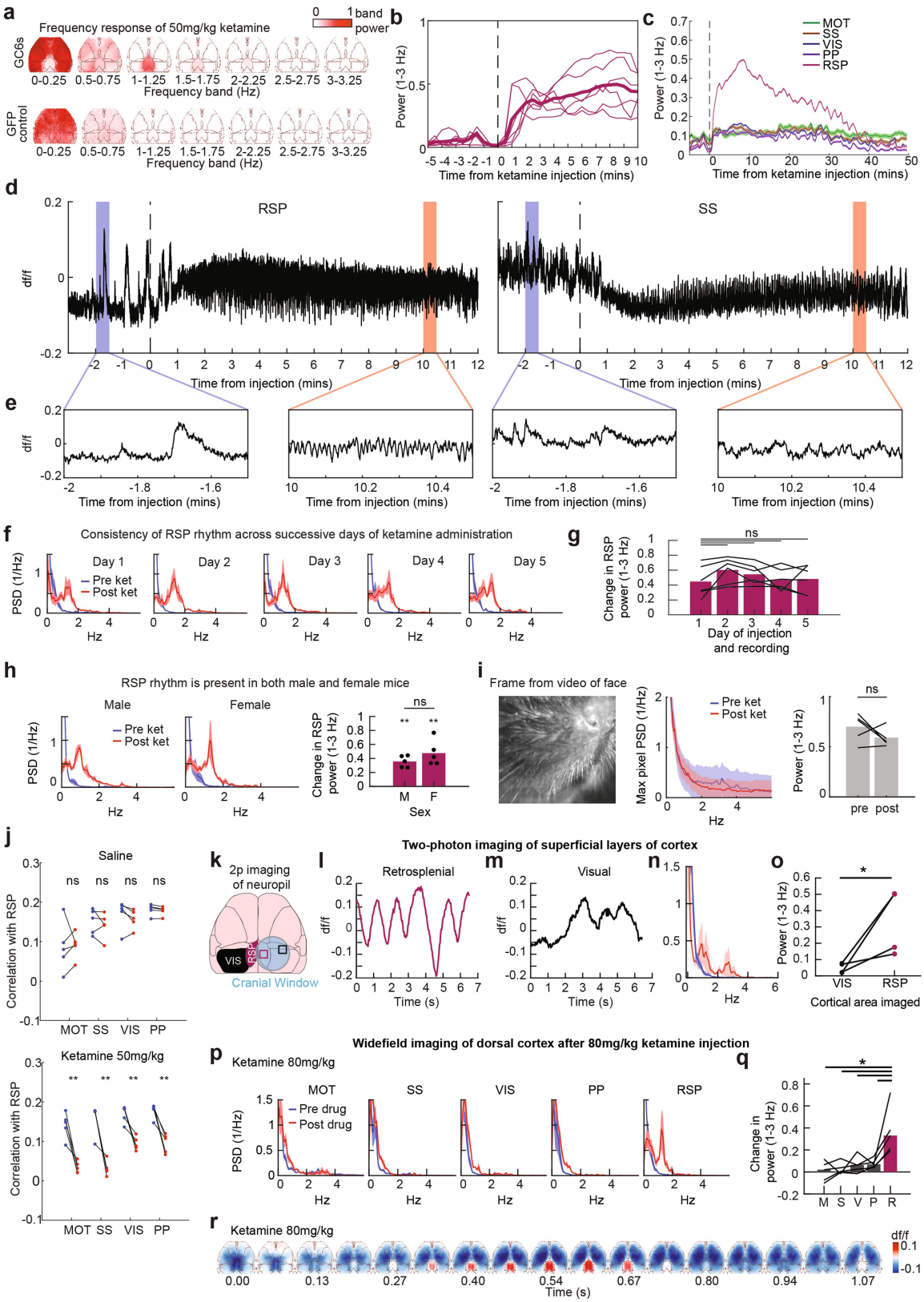

Extended Data Fig. 1 | See next page for caption.

Extended Data Fig. 1 | Time course of ketamine-induced retrosplenial rhythm. a, Prominent 1–3 Hz retrospenial activity after ketamine injection seen in a frequency response from Thy1-GCaMP6s (top) but not control (Thy1–GFP) mice (bottom). **b**, Expansion of the first 15 min of the recording shown in Fig. 1g. **c**, Power in 1–3 Hz band in motor (MOT), somatosensory (SS), visual (VIS), posterior parietal (PP) and retrosplenial (RSP) cortices (mean ± s.e.m., $n = 6$ mice). **d**, Example 410-nm channel-corrected trace of RSP and SS activity from 3 min before to 12 min after intraperitoneal injection of 50 mg kg^{-1} ketamine. Vertical lines indicate injection time. **e**, Magnifications of 30 s of data demonstrating oscillatory rhythm in the RSP but not the SS at ten minutes after injection, or before injection. **f**, PSD in the RSP during five consecutive days of 50 mg kg^{-1} ketamine injection (mean ± s.e.m., $n = 6$ mice). **g**, Summary of power in the 1–3 Hz band in the RSP during five consecutive days of 50 mg kg^{-1} ketamine injection (ns, corrected paired t-test comparison with first day, $P = 0.10, 0.10, 0.80, 0.75$, Hedge's $g = 0.73, 0.49, 0.12, 0.15$). **h**, Direct comparison of oscillation in similarly aged male and female mice. PSD in the RSP and summary of power in the 1–3 Hz band. Both sexes have significant increase in power relative to pre-injection, but the magnitude is not significantly different between male and female mice ($P < 0.01$, corrected t-test versus 0, and $P = 0.21$, t-test between groups, Hedge's $g = 0.76$). **i**, Video tracking of mouse facial movements. Facial movements did not show 1–3 Hz features before or after administration of ketamine (paired t-test $P = 0.24$, Hedge's $g = 0.80$). **j**, Top, correlation of cortical areas imaged with widefield imaging, before and after saline injection ($n = 5$ mice, corrected paired t-test $P = 0.85, 0.51, 0.37, 0.25$, Hedge's $g = 0.08, 0.27, 0.36, 0.21$). Bottom, correlation of cortical areas imaged with widefield imaging, before and after injection of 50 mg kg^{-1} ketamine ($n = 5$ mice, corrected paired t-test $P = 0.009, 0.009, 0.009, 0.009$, Hedge's $g = 3.88, 3.67, 3.75, 3.39, 3.36$). **k**, Schematic of cranial window preparation and two-photon imaging of superficial neuropil. **l**, Example fullfield fluorescence trace from the RSP in a ketamine-injected Thy1-GCaMP6s mouse, imaged 30 µm below the cortical surface. **m**, Example fullfield fluorescence trace from the visual cortex, in the same mouse (same ketamine injection as in **l**). **n**, Quantification of oscillation frequency content from neuropil in cortical surface before (blue) and after (red) ketamine injection, $n = 4$ mice. **o**, Comparison of mean power in the 1–3 Hz band after ketamine injection; $n = 4$ mice (one-sided paired t-test, $P = 0.035$; Hedge's $g = 1.60$). **p**, Quantification of oscillation frequency content before and after injection of 80 mg kg^{-1} ketamine, $n = 5$ mice; solid line represents the mean and shading denotes the s.e.m. **q**, After injection of 80 mg kg^{-1} ketamine, comparison of mean power in the 1–3 Hz band, $n = 5$ mice. One-way ANOVA with repeated measures, $F_{4,16} = 3.74$, $P = 0.025$. Corrected two-sided paired t-tests $P = 0.016, 0.034, 0.016, 0.034$; Hedge's g 1.92, 1.90, 1.66, 1.65. **r**, After injection of 80 mg kg^{-1} ketamine, example temporal video sequence of 410 nm-corrected fluorescence over 1 s in a Thy1-GCaMP6s mouse. A prominent rhythm is seen in the RSP.

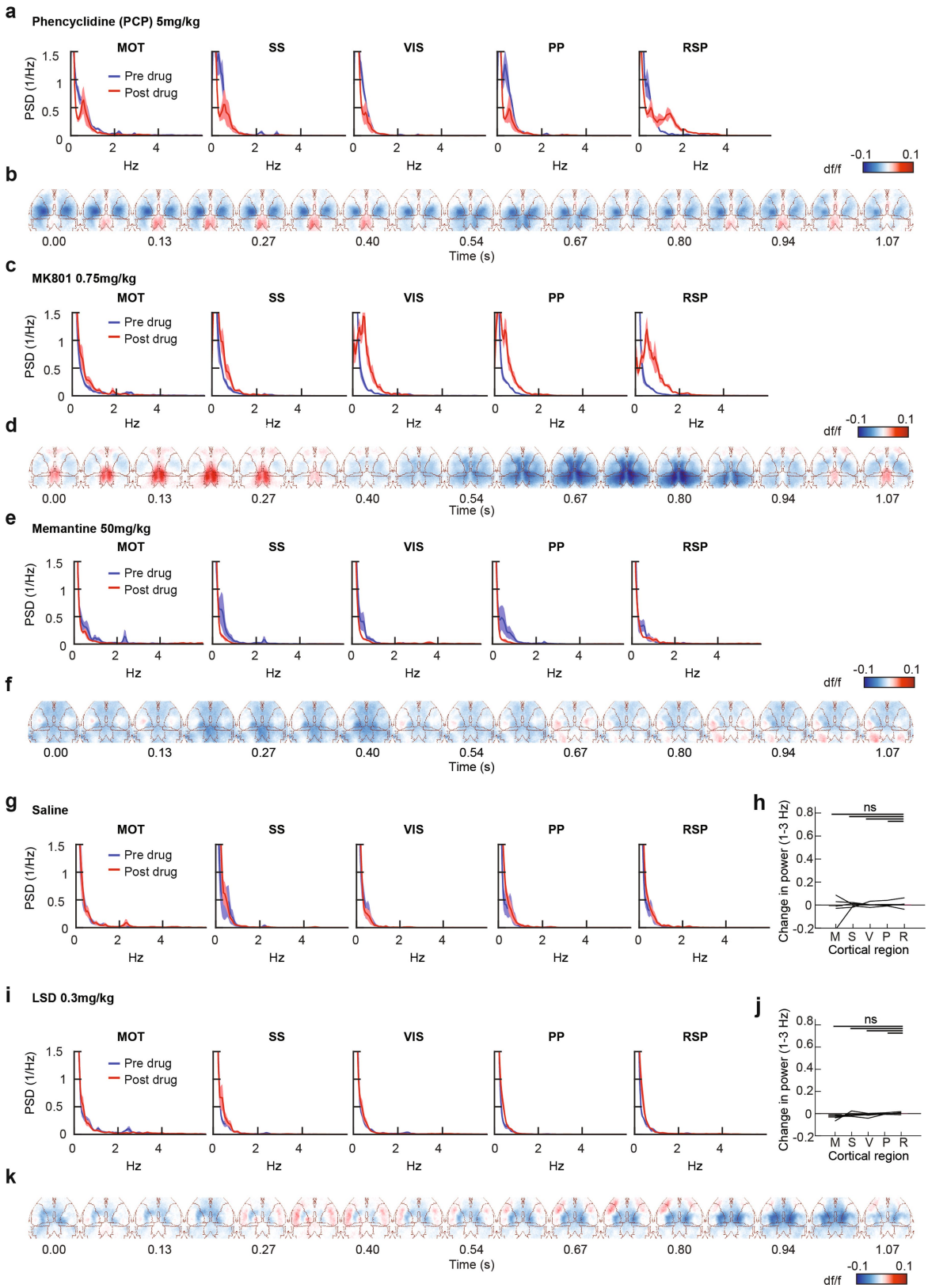

Extended Data Fig. 2 | See next page for caption.

Extended Data Fig. 2 | PCP and MK801—but not memantine, saline or LSD—induce RSP-localized rhythms. a, Quantification of oscillation frequency content before and after PCP injection, $n = 5$ mice. **b**, For PCP, example temporal video sequence of 410 nm-corrected fluorescence over 1 s in a Thy1-GCaMP6s mouse showing RSP rhythm. **c**, Quantification of oscillation frequency content before and after MK801 injection, $n = 5$ mice. **d**, For MK801, example temporal video sequence of 410 nm-corrected fluorescence over 1 s in a Thy1-GCaMP6s mouse, showing RSP rhythm. **e**, Quantification of oscillation frequency content before and after memantine injection, $n = 5$ mice. **f**, For memantine, example temporal video sequence of 410 nm-corrected fluorescence across 1 s in a Thy1-GCaMP6s mouse. Here, neither rhythms nor travelling waves are seen. **g**, Quantification of oscillation frequency content before and after saline injection, $n = 5$ mice. **h**, Quantification of mean power in 1–3 Hz band for saline ($n = 5$ mice), corrected two-sided paired *t*-tests (*$P < 0.05$, **$P < 0.01$, NS $P > 0.05$; Hedge's *g* 0.36, 0.18, 0.14, 0.01). **i**, Quantification of oscillation frequency content before and after LSD injection, $n = 5$ mice. **j**, Quantification of mean power in 1–3 Hz band for LSD ($n = 5$ mice), corrected two-sided paired *t*-tests (*$P < 0.05$, **$P < 0.01$, NS $P > 0.05$; Hedge's *g* LSD 2.05, 0.62, 1.07, 0.65). **k**, For LSD, example temporal video sequence of 410 nm-corrected fluorescence across 1 s in a Thy1-GCaMP6s mouse. Here, neither rhythms nor travelling waves are seen.

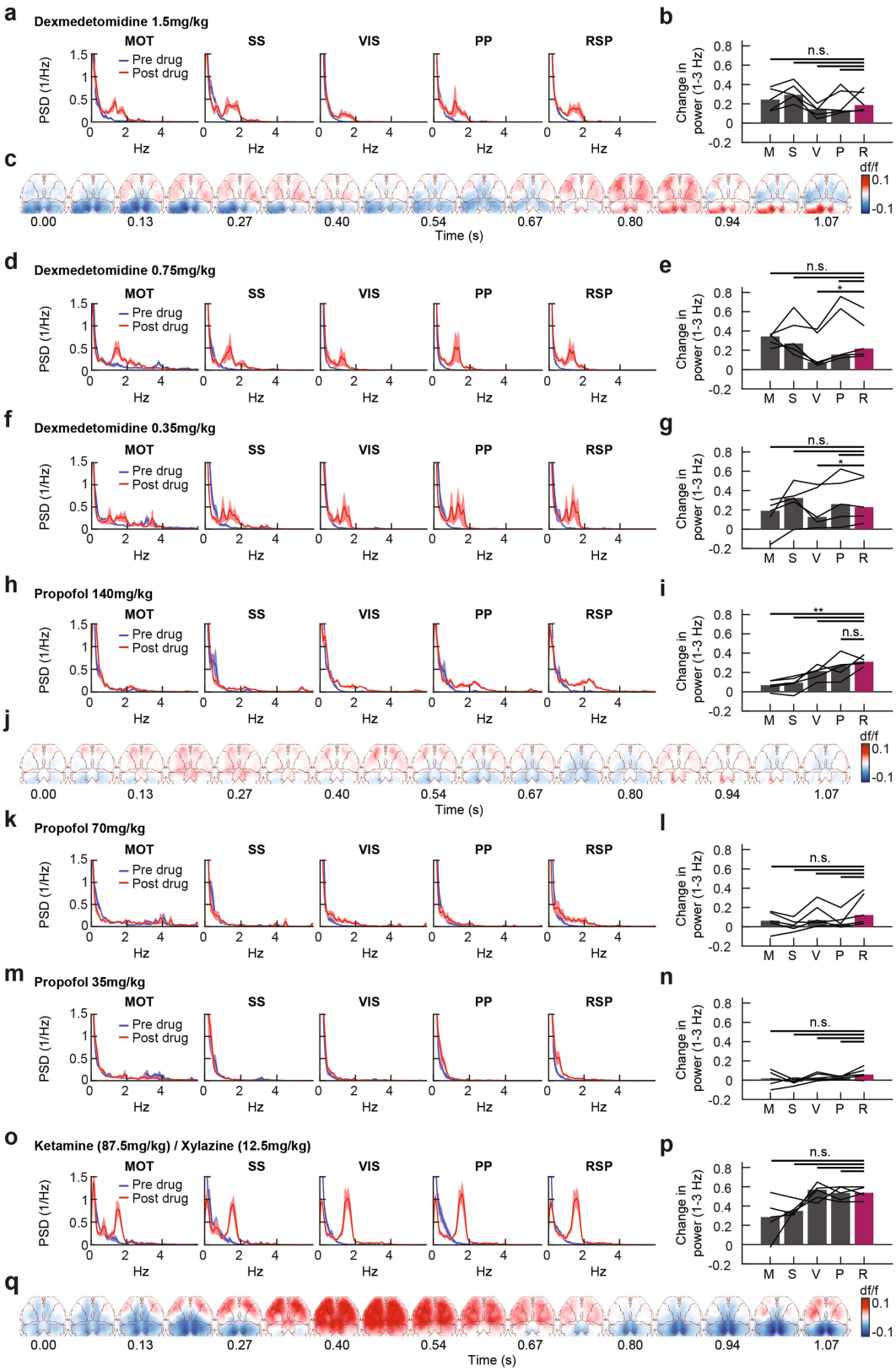

Extended Data Fig. 3 | See next page for caption.

Extended Data Fig. 3 | Other anaesthetic classes do not induce retrosplenial cortex-localized rhythms. a, Quantification of oscillation frequency content before and after injection of 1.5 mg kg^{-1} dexmedetomidine, $n = 5$ mice. **b**, After injection of 1.5 mg kg^{-1} dexmedetomidine, comparison of mean power in the 1–3 Hz band, $n = 5$ mice. One-way ANOVA with repeated measures, $F_{4,16} = 2.66$, $P = 0.07$. Corrected two-sided paired *t*-tests, $P = 0.91, 0.27, 0.15, 0.91$; Hedge's $g = 0.14, 0.77, 1.01, 0.06$. **c**, Example temporal video sequence of 410 nm-corrected fluorescence after injection of 1.5 mg kg^{-1} dexmedetomidine over 1 s in a Thy1-GCaMP6s mouse. **d**, Quantification of oscillation frequency content before and after injection of 0.75 mg kg^{-1} dexmedetomidine, $n = 5$ mice. **e**, After injection of 0.75 mg kg^{-1} dexmedetomidine, comparison of mean power in the 1–3 Hz band, $n = 5$ mice. One-way ANOVA with repeated measures, $F_{4,16} = 2.340$, $P = 0.10$. Corrected two-sided paired *t*-tests, $P = 0.92, 0.92, 0.04, 0.86$; Hedge's $g = 0.05, 0.11, 0.54, 0.13$. **f**, Quantification of oscillation frequency content before and after injection of 0.35 mg kg^{-1} dexmedetomidine, $n = 5$ mice. **g**, After injection of 0.35 mg kg^{-1} dexmedetomidine, comparison of mean power in the 1–3 Hz band, $n = 5$ mice. One-way ANOVA with repeated measures, $F_{4,16} = 2.68$, $P = 0.07$. Corrected two-sided paired *t*-tests, $P = 0.29, 0.95, 0.013, 0.95$; Hedge's $g = 0.68, 0.05, 0.32, 0.01$. **h**, Quantification of oscillation frequency content before and after injection of 140 mg kg^{-1} propofol, $n = 5$ mice. **i**, After injection of 140 mg kg^{-1} propofol, comparison of mean power in the 1–3 Hz band, $n = 5$ mice. One-way ANOVA with repeated measures, $F_{4,16} = 6.46$, $P = 0.0027$. Corrected two-sided paired *t*-tests, $P = 0.0026, 0.0029, 0.0029, 0.28$; Hedge's $g = 4.36, 3.07, 1.75, 0.61$. **j**, Example temporal video sequence of 410 nm-corrected fluorescence after injection of 140 mg kg^{-1} propofol over 1 s in a Thy1-GCaMP6s mouse. **k**, Quantification of oscillation frequency content before and after injection of 70 mg kg^{-1} propofol, $n = 5$ mice. **l**, After injection of 70 mg kg^{-1} propofol, comparison of mean power in the 1–3 Hz band, $n = 5$ mice. One-way ANOVA with repeated measures, $F_{4,16} = 1.34$, $P = 0.30$. Corrected two-sided paired *t*-tests, $P = 0.11, 0.11, 0.11, 0.11$; Hedge's $g = 0.79, 1.17, 0.37, 0.83$. **m**, Quantification of oscillation frequency content before and after injection of 35 mg kg^{-1} propofol, $n = 5$ mice. **n**, For injection of 35 mg kg^{-1} propofol, comparison of mean power in the 1–3 Hz band, $n = 5$ mice. One-way ANOVA with repeated measures, $F_{4,16} = 2.69$, $P = 0.07$. Corrected two-sided paired *t*-tests, $P = 0.17, 0.07, 0.07, 0.17$; Hedge's $g = 0.66, 1.56, 0.63, 0.82$. **o**, Quantification of oscillation frequency content before and after injection of ketamine/xylazine, $n = 5$ mice. **p**, After injection of ketamine/xylazine, comparison of mean power in the 1–3 Hz band, $n = 5$ mice. One-way ANOVA with repeated measures, $F_{4,16} = 1.977$, $P = 0.15$. Corrected two-sided paired *t*-tests, $P = 0.08, 0.08, 0.82, 0.82$; Hedge's $g = 1.44, 2.25, 0.08, 0.13$. **q**, Example temporal video sequence of 410 nm-corrected fluorescence after injection of ketamine/xylazine over 1 s in a Thy1-GCaMP6s mouse.

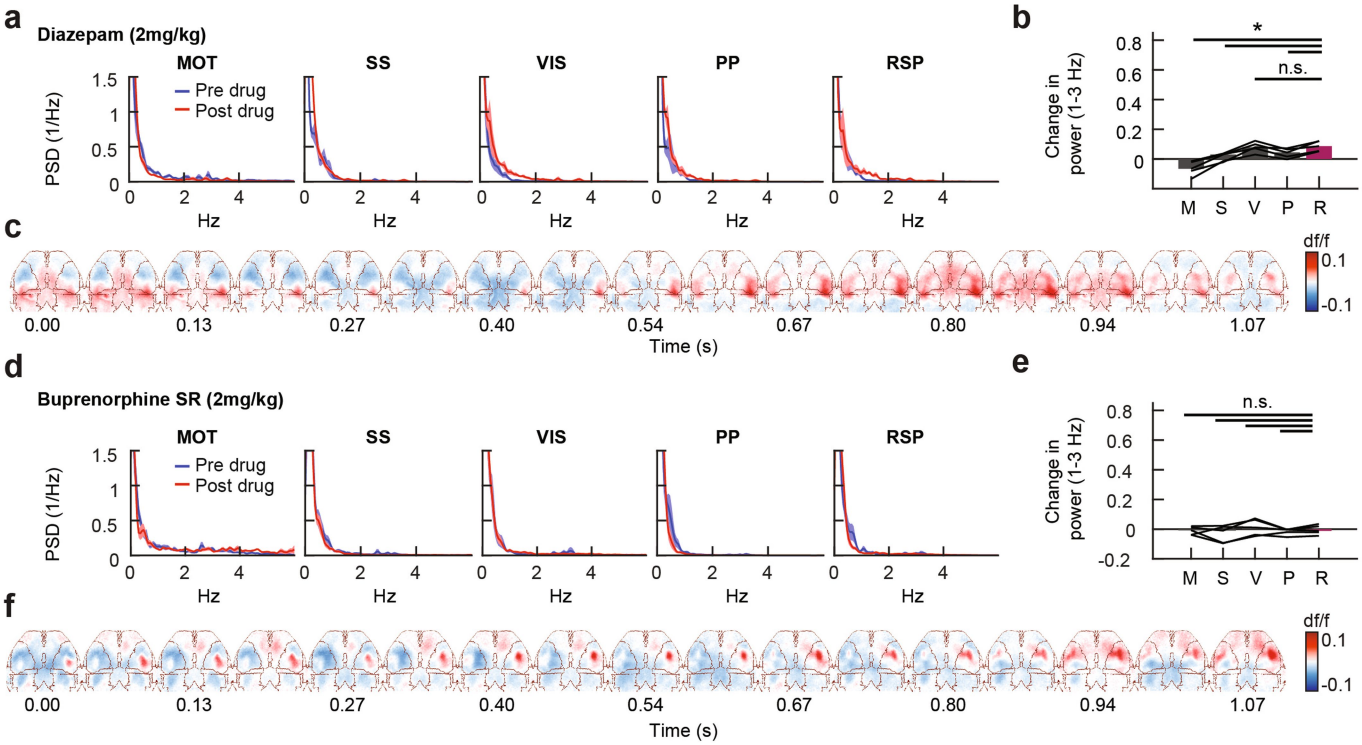

Extended Data Fig. 4 | A sedative and an analgesic do not induce the retrosplenial rhythm. a, Quantification of oscillation frequency content before and after injection of 2 mg kg^{-1} diazepam, $n = 5$ mice. **b**, After injection of 2 mg kg^{-1} diazepam, comparison of mean power in the 1–3 Hz band, $n = 5$ mice. One-way ANOVA with repeated measures, $F_{4,16} = 39$, $P < 0.001$. Corrected two-sided paired *t*-tests, $P = 0.013, 0.028, 0.67, 0.013$; Hedge's $g = 3.10, 2.07, 0.16, 1.27$. **c**, Example temporal video sequence of 410 nm-corrected fluorescence after injection of 2 mg kg^{-1} diazepam over 1 s in a Thy1-GCaMP6s mouse. **d**, Quantification of oscillation frequency content before and 2 h after injection of buprenorphine SR, $n = 5$ mice. **e**, After injection of buprenorphine SR, comparison of mean power in the 1–3 Hz band, $n = 5$ mice. One-way ANOVA with repeated measures, $F_{4,16} = 1.55$, $P = 0.23$. Corrected two-sided paired *t*-tests, $P = 0.51, 0.33, 0.33, 0.33$; Hedge's $g = 0.17, 0.51, 0.33, 0.38$. **f**, Example temporal video sequence of 410 nm-corrected fluorescence after injection of buprenorphine SR, over 1 s in a Thy1-GCaMP6s mouse.

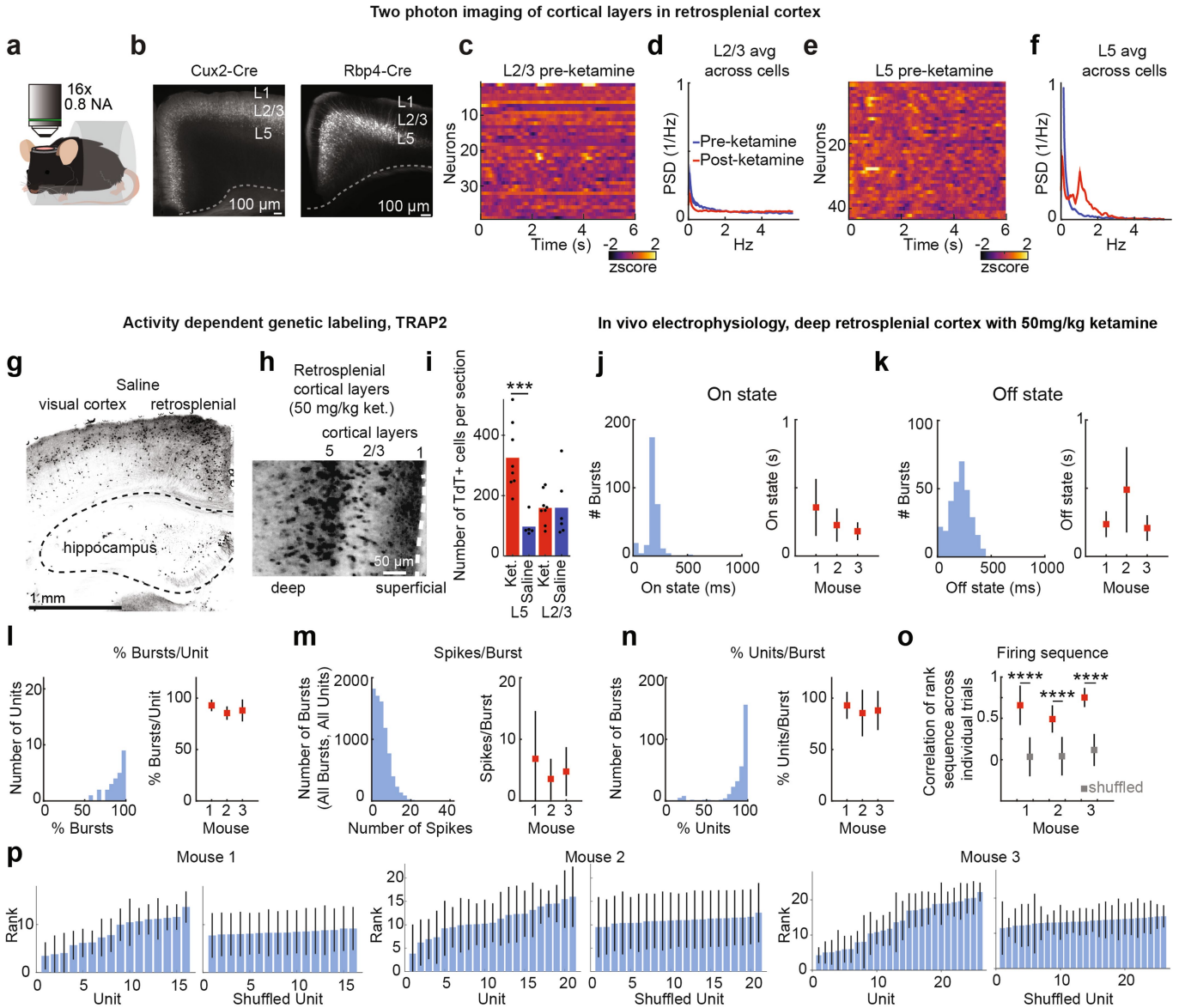

Extended Data Fig. 5 | Additional information for two photon imaging, TRAP and 32-contact electrophysiology experiments. a, Schematic of two-photon, head-fixed imaging. GCaMP6m was expressed in layer-specific transgenic mice, and a cranial window was placed over the RSP. **b**, Epifluorescence images of coronal sections showing GCaMP6m expression restricted to either layer 2/3 or layer 5 neurons in the RSP. Scale bar, 100 µm. **c**, Single-cell activity traces of all recorded layer 2/3 retrosplenial neurons before ketamine injection, from one mouse. **d**, Quantification of oscillation frequency content in single layer 2/3 cells before and after ketamine injection, data show average and s.e.m. from $n = 5$ mice. **e**, Single-cell activity traces of all recorded layer 5 retrosplenial neurons before ketamine injection from one mouse. **f**, Quantification of oscillation frequency content in single layer 5 cells before and after ketamine injection, data show average and s.e.m. from $n = 5$ mice. **g**, Fluorescence images showing tdTomato expression after recombination of TRAP2;Ai14 mice, after saline injections. Scale bar, 1 mm. **h**, Magnified example image of the RSP after ketamine injection. Dense labelling (tdTomato$^+$ neurons are black cells) in deep layers is observed. **i**, Quantification of tdTomato$^+$ induction in the RSP in TRAP2;Ai14 mice after saline (blue, $n = 6$ coronal sections) or ketamine (red, $n = 8$ coronal sections) injections. Two-sided unpaired t-test, layer 2/3, $P = 0.42$; layer 5, $P < 0.0004$; Hedge's $g = 2.42$. **j**, Left, histogram of spike rate during ON periods for mouse 3. Right, summary plot for three mice. **k**, Left, histogram of spike rate during OFF periods for mouse 3. Right, summary plot for three mice. **l**, Quantification of the percentage of recorded units that participated in each burst. Left, histogram of per cent units participating in a burst from mouse 3 ($n = 249$ bursts). Right, summary plot for three mice. **m**, Quantification of the number of spikes in each burst. Left, histogram from mouse 3. Right, summary plot for three mice. **n**, Quantification of the percentage of bursts that each neuron participates in. Left, histogram from mouse 3. Right, summary plot for three mice. **o**, For all 3 mice, correlation of rank sequence across all bursts over 2 min, compared to shuffling of unit IDs. Two-sided paired t-test, $P < 0.0001$ for all mice. The box denotes the mean and the bars the s.e.m. Hedge's $g = 2.30, 2.25, 3.93$. **p**, Temporal organization of firing across bursts for each mouse. Left, rank of each neuron's first spike in burst (averaged across bursts for each neuron). Right, rank of each neurons first spike with shuffling of unit IDs.

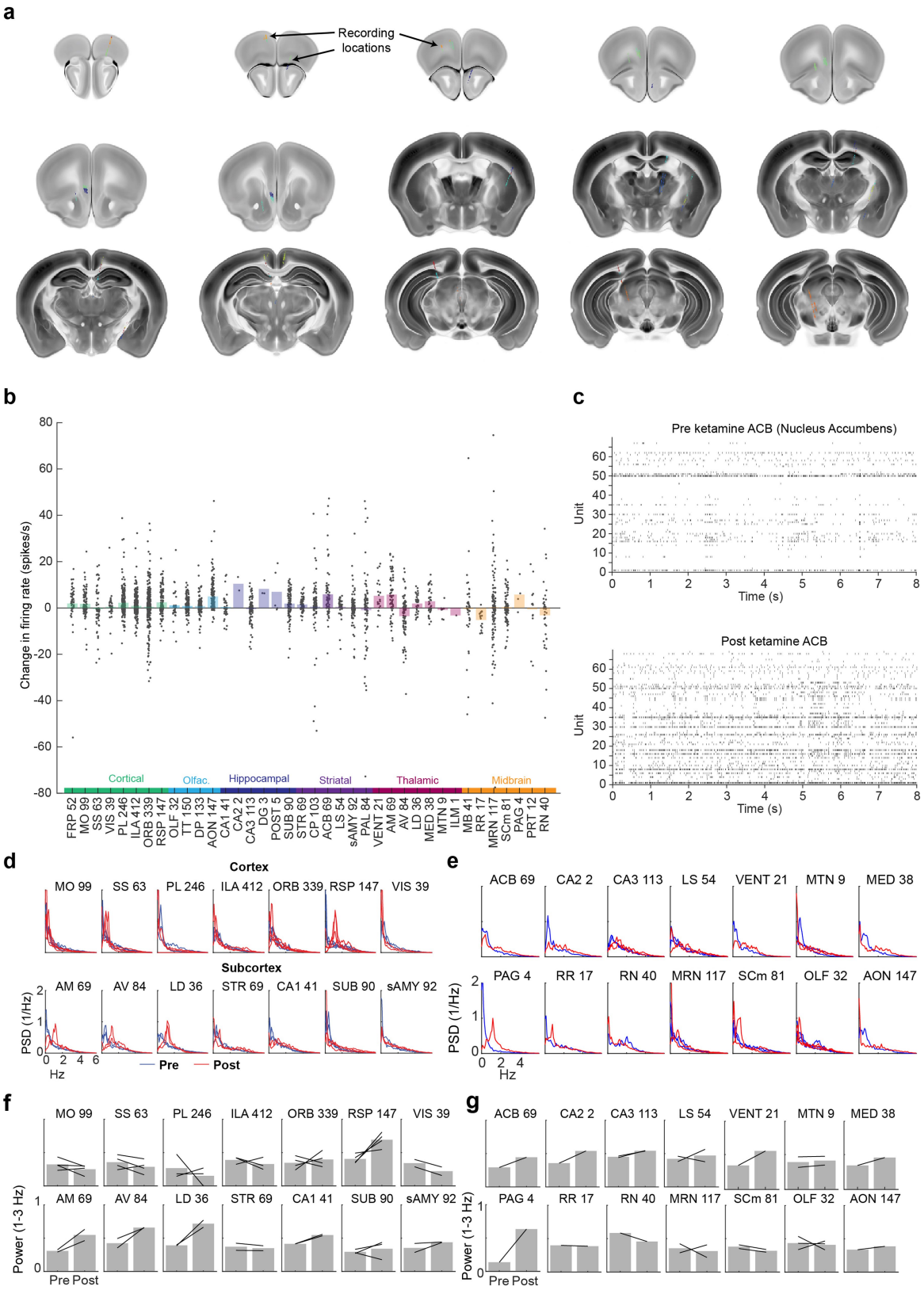

Extended Data Fig. 6 | Brain-wide single-cell firing rates and spectral features. a, Recording locations overlaid on coronal sections from the Allen Mouse Brain Atlas. **b**, Change in firing rate per brain region between 8–12 min before and 8–12 min after ketamine injection, each grey dot is an individual cell. Cells from all 4 sessions are included. **c**, Nucleus accumbens spike rasters before (top) and after (bottom) ketamine injection from a single session. **d**, PSD plots for cortical and subcortical regions in Fig. 2d–f; before (blue) and after (red) ketamine injection. **e**, PSD plots for additional subcortical regions; before (blue) and after (red) ketamine injection. **f**, Average regional power in the 1–3Hz band for cortical and subcortical regions from **d**. Each recording is represented as a single line. The total number of recorded units is indicated. **g**, Average regional power in the 1–3Hz band for additional subcortical regions from **e**. Each recording is represented as a single line. The total number of recorded units is indicated.

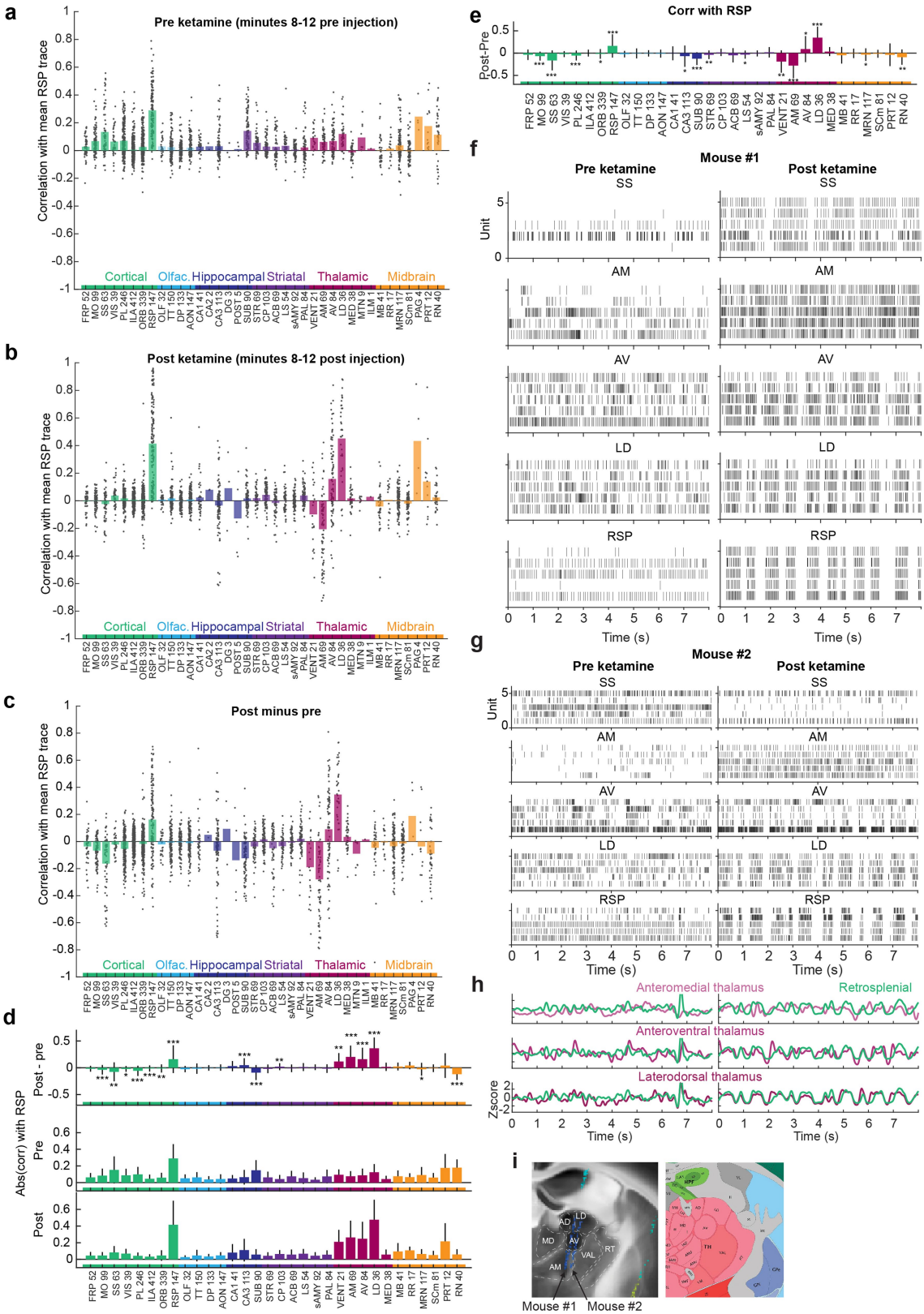

Extended Data Fig. 7 | See next page for caption.

Extended Data Fig. 7 | Brain-wide functional correlations with retrosplenial cortex and thalamic rhythms. a, Before ketamine infusion, correlation with the average RSP trace for every recorded cell (grey dot) categorized by region. **b**, After ketamine infusion, correlation with the average RSP trace for every recorded cell (grey dot) categorized by region. **c**, For every neuron, change in correlation with the mean RSP trace. **d**, For every region, magnitude of correlation with the mean RSP trace. **e**, For every region, change in the correlation with mean RSP trace. Regional averages (bar) and s.e.m (line) are shown. **f**, For mouse 1, raster plot of spike trains from simultaneously recorded single units in somatosensory cortex (SS), anteromedial thalamus (AM), anteroventral thalamus (AV), lateral dorsal thalamus (LD) and retrosplenial cortex (RSP) before and after ketamine injection. **g**, For mouse 2, raster plot of spike trains from simultaneously recorded single units in somatosensory cortex (SS), anteromedial thalamus (AM), anteroventral thalamus (AV), lateral dorsal thalamus (LD) and retrosplenial cortex (RSP) before and after ketamine injection. **h**, *Z*-scored mean activity traces from three simultaneously recorded thalamic nuclei and retrosplenial cortex (green) corresponding to rasters in **f**. **i**, Histological assessment registered to the Allen Mouse Brain Atlas (2004)[49]. Electrode insertions revealed the location of mouse 2's thalamic probe at the edge of the anteromedial thalamus, a possible explanation for this recording's fewer AM neurons and weaker anti-correlation with RSP. Right, a coronal image from the Allen Mouse Brain Atlas shows the locations of thalamic nuclei.

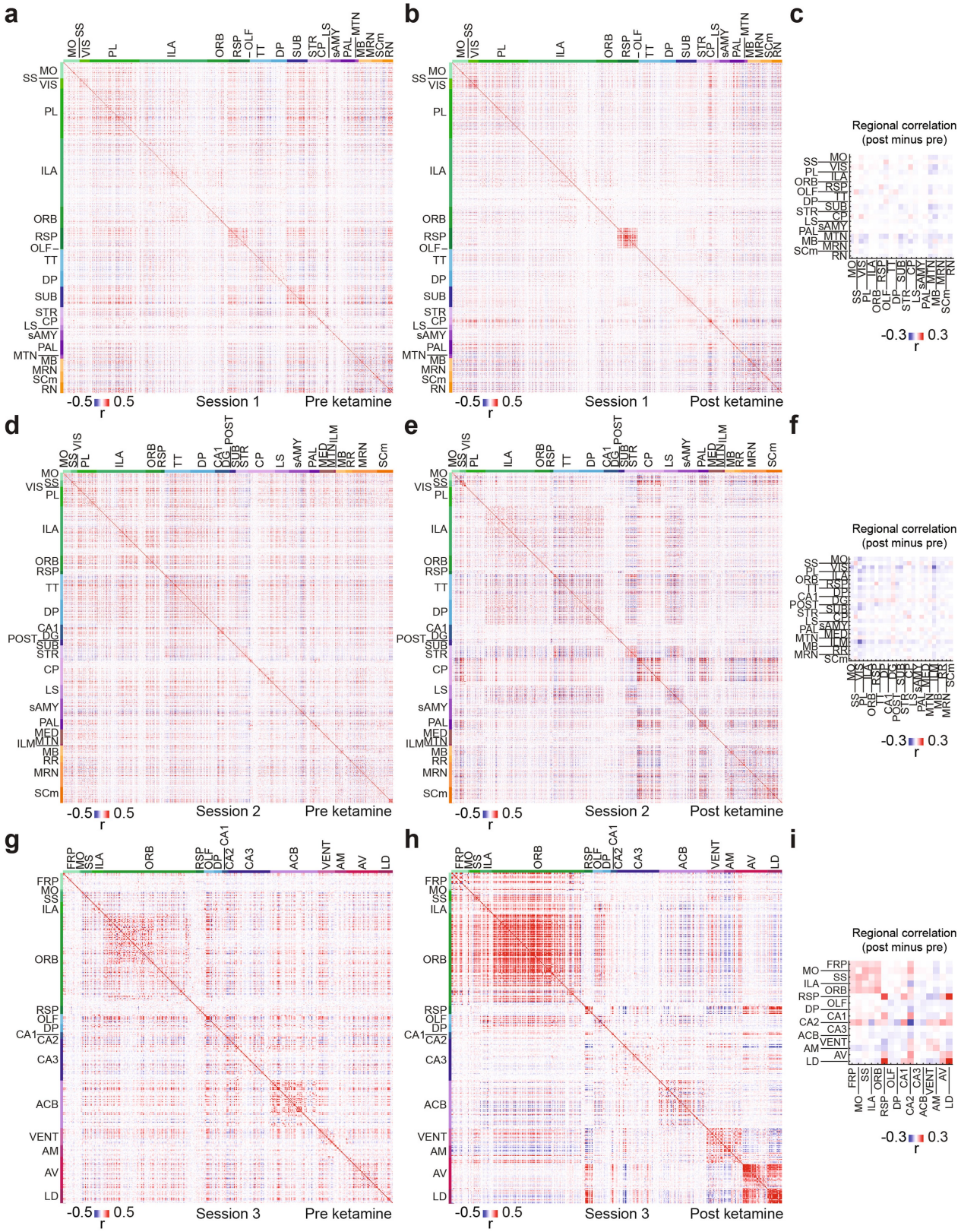

Extended Data Fig. 8 | Brain-wide single-cell functional connectivity matrices. a, Correlation matrix between individual cells, grouped by brain region, before ketamine infusion for recording session 1. **b**, Correlation matrix between individual cells, grouped by brain region, after ketamine infusion for recording session 1. **c**, Change in regional correlation for recording session 1. **d**, Correlation matrix between individual cells, grouped by brain region, before ketamine infusion for recording session 2. **e**, Correlation matrix between individual cells, grouped by brain region, after ketamine infusion for recording session 2. **f**, Change in regional correlation for recording session 2. **g**, Correlation matrix between individual cells, grouped by brain region, before ketamine infusion for recording session 3. **h**, Correlation matrix between individual cells, grouped by brain region, after ketamine infusion for recording session 3. **i**, Change in regional correlation for recording session 3.

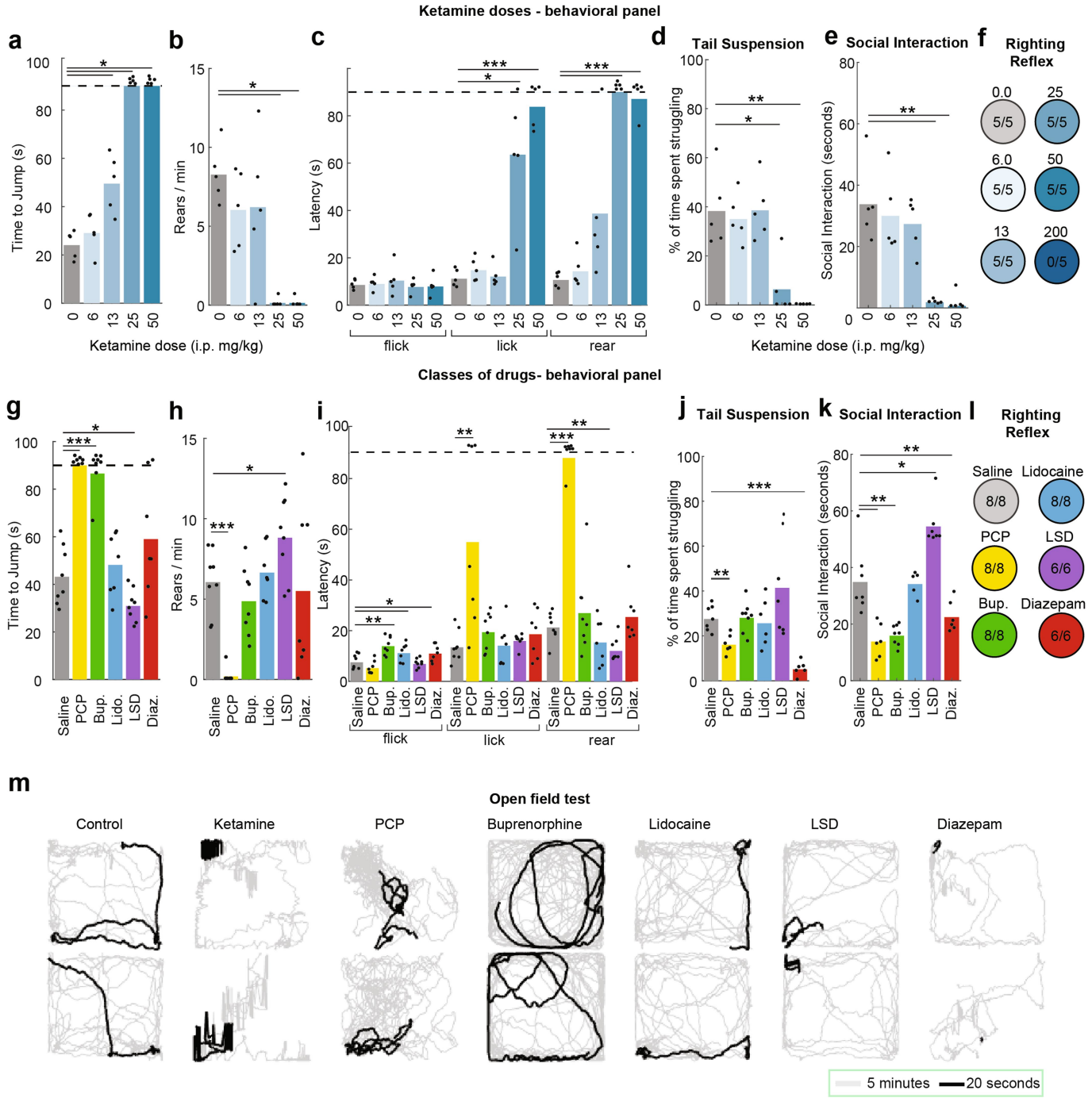

Extended Data Fig. 9 | See next page for caption.

Extended Data Fig. 9 | Additional characterization of dissociation-like phenotype elicited by ketamine and PCP. a, Hot-plate test. Time to jump in ketamine-injected mice. The maximum allowable test time was 90 s. One-way ANOVA with repeated measures: jump, 1×10^{-12}. Horizontal dotted line indicates the experimental time limit; mice that did not jump by 90 s were removed and the experiment ended. Corrected two-sided unpaired *t*-tests, $^{*}P < 0.05$, $^{**}P < 0.01$, $^{***}P < 0.001$. $n = 5$ mice in each group. For each dose in order, Glass's Δ effect size for jump = 0.55, 1.9, Inf, Inf. **b**, Rate of rears in hot-plate test. One-way ANOVA with repeated measures, $P < 1 \times 10^{-4}$. Two-sided unpaired *t*-tests. For each dose in order, Glass's Δ effect sizes = −0.82, −0.42, −24.6, −24.6. **c**, Latency to first flick, lick and rear in hot-plate test. The horizontal dotted line indicates the experimental time limit. Hedge's *g* effect sizes for flick = 0.16, 0.34, −0.30, −0.17. Glass's Δ effect size for lick = 0.66, 0.17, 1.86, 7.62. Glass's Δ effect size for rear = 0.47, 0.85, Inf, 10.5. **d**, Tail suspension test. Percentage of time spent struggling. One-way ANOVA with repeated measures, $F_{4,20} = 9.36$, $P = 0.0002$, $n = 5$ mice for each group. Glass's Δ effect sizes = −0.30, 0.024, −2.49, −585. **e**, Time spent interacting with an intruder mouse in 2 min. One-way ANOVA with repeated measures, $F_{4,20} = 15.8$; $P < 0.0001$, $n = 5$ mice for each group. Glass's Δ effect sizes = −0.27, −0.67, −44.7, −79.5. **f**, Number of mice that corrected postural inversion within 5 s. Mice dosed with 50 mg kg^{-1} ketamine or less reflexively righted. Mice injected with 200 mg kg^{-1} ketamine did not right. $n = 5$ for each group. **g**, Hot-plate test, time to jump. The maximum allowable time is indicated by a dashed horizontal line (90 s); mice that did not jump by 90 s were removed and the experiment ended. For all statistical comparisons, each experimental group was compared with the saline (control) group via corrected Mann–Whitney *U*-test. $^{*}P < 0.05$, $^{**}P < 0.01$, $^{***}P < 0.001$; for each drug in order, Glass's Δ effect size for jump = Inf, 4.97, 0.35, −1.69, 0.60. **h**, Rearing rate was significantly decreased for the PCP group and increased for the LSD group. Glass's Δ = −10.9, −0.52, 0.34, 1.00, −0.10. **i**, Latencies to expression of affective (licking) and escape (rear) behaviours were significantly longer for the PCP mice. The maximum allowable time is indicated by dashed horizontal line (90 s). Hedge's *g* effect sizes for flick = −0.78, 1.87, 1.07, −0.24, 1.05. Glass's Δ effect size for lick = 1.14, 0.75, 0.072, 0.96, 0.52. Glass's Δ effect size for rear = 12.4, 0.33, −0.63, −1.92, 0.39. **j**, Tail suspension test. Significantly decreased struggling time was observed in mice treated with PCP and diazepam compared with saline-injected mice (Mann–Whitney *U*-test with FDR correction, $^{**}P < 0.01$). Glass's Δ effect sizes = −2.51, 0.074, −0.17, 0.58, −6.50. **k**, Social interaction. Significantly decreased social interaction time was observed in mice treated with PCP and buprenorphine (Mann–Whitney *U*-test with FDR, $^{**}P < 0.01$). Hedge's *g* effect sizes = −2.10, −2.13, −0.068, 1.88, −1.23. **l**, Righting reflex, showing the number of mice that right for each treatment group. For each group, all mice successfully corrected postural inversion. **m**, Open field test. Example traces of body position after treatment with each drug (2 example mice shown). Grey line represents full 5-min session, black line represents 20 s of tracking (from 2 min to 2 min 20 s).

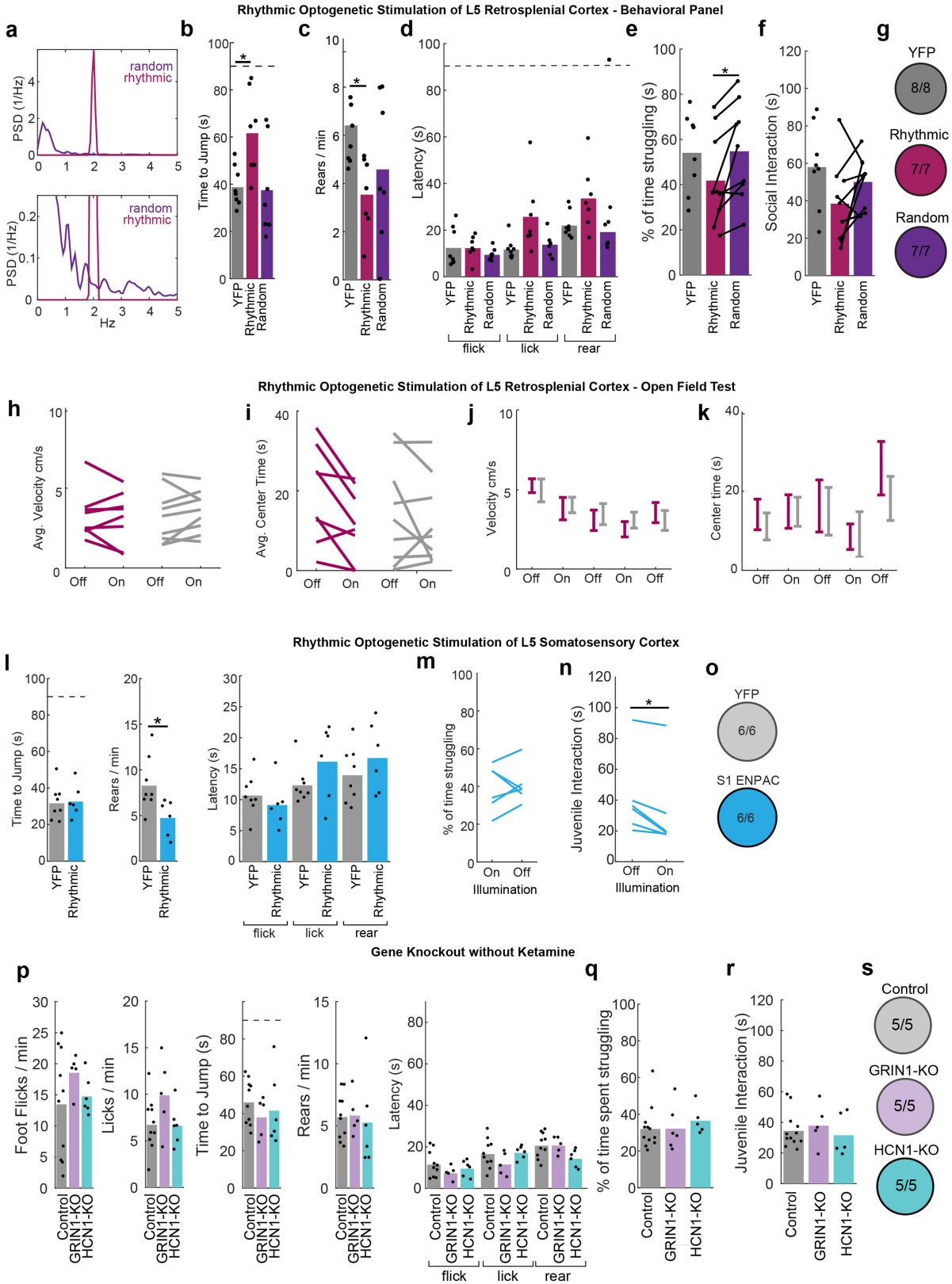

Extended Data Fig. 10 | See next page for caption.

Extended Data Fig. 10 | Rhythmic optogenetic behaviour, alternative cortical stimulation locations, and behavioural controls. a, Frequency content of rhythmic (magenta) and random (purple) illumination patterns. **b**, Hot-plate test: time to jump. The maximum allowable time is indicated by dashed horizontal line (90 s). Time-to-jump: YFP/rhythmic $P = 0.020$, YFP/random $P = 0.87$, rhythmic/random $P = 0.054$, corrected two-sided unpaired *t*-tests, $n = 8$ YFP, 7 rhythmic, 7 random mice. Hedge's *g* effect sizes for jump = 1.58, −0.79, −1.2). **c**, Rate of rears, two-sided unpaired *t*-test, YFP/rhythmic $P = 0.020$, YFP/random $P = 0.27$, rhythmic/random $P = 0.44$. Hedge's *g* effect sizes = −1.57, −0.68, −0.40. **d**, Latency to first withdrawal, lick and rear. The maximum allowable time is indicated by the dashed horizontal line (90 s). Two-sided unpaired *t*-tests, corrected *P* values for foot flick (>0.5 for all comparisons); foot lick: YFP/rhythmic $P = 0.087$, YFP/random $P = 0.40$, rhythmic/random $P = 0.12$; rear: $P = 0.071$, 0.42, 0.071; Hedge's *g* effect sizes for flick = −0.0084, −0.43, −0.66; lick = 1.20, 0.42, −0.97; and rear = 1.07, −0.42, −1.2. **e**, Tail suspension test. Two-sided paired *t*-test for rhythmic/random, corrected $P = 0.038$; Two-sided unpaired *t*-tests: YFP/rhythmic corrected $P = 0.31$ and YFP/rand corrected $P = 0.95$. Hedge's *g* effect sizes: YFP/rhythmic −0.61, rhythmic/random −0.58, YFP/random 0.032. **f**, Social interaction. Two-sided paired *t*-test for rhythmic/random, corrected $P = 0.21$; Two-sided unpaired *t*-tests: YFP/rhythmic corrected $P = 0.21$ and YFP/random corrected $P = 0.39$. Hedge's *g* effect sizes: YFP/rhythmic = −0.85, rhythmic/random = 0.60, YFP/random = −0.42. **g**, Righting reflex, percentage of mice that right. In each group, all mice successfully corrected postural inversion. **h**, Average velocity in the open field test during optogenetic stimulation, comparing average light off and light on conditions within individual mice. Paired *t*-test, eNPAC $P = 0.49$, YFP $P = 0.40$. **i**, Time in centre in the open field test, comparing average light off and light on conditions within individual mice. Paired *t*-test, eNPAC $P = 0.06$, YFP $P = 0.25$. **j**, Velocity for each 3 min epoch. eNPAC (magenta) and YFP (grey). s.e.m. is shown. **k**, Time in centre for each 3 min epoch. eNPAC (magenta) and YFP (grey). s.e.m. is shown. **l**, Hot-plate test. Rate of jumps ($P = 0.85$), rearing ($P = 0.03$) and latencies. Two-sided paired *t*-test, $n = 8$ control mice and $n = 6$ S1 eNPAC mice. Hedge's *g* effect size for jump = 0.09, rear = −1.27, latency to flick = −0.41, latency to lick = 0.78, latency to rear = 0.52. **m**, Tail suspension test. Percentage of time spent struggling for S1 eNPAC mice, with and without illumination, two-sided paired *t*-test, $P = 0.73$. Change in struggling time, $P = 0.73$. Hedge's $g = 0.11$. **n**, Social interaction. Interaction time significantly decreased with illumination in S1 eNPAC mice, two-sided paired *t*-test, $P = 0.015$; percentage change with illumination. Hedge's $g = -0.29$. **o**, Righting reflex for S1 YFP and ENPAC mice. **p**, Hot-plate test without ketamine. For rate of reflexive withdrawals (one-way ANOVA, $F_{2,18} = 1.01$, $P = 0.38$), paw-licks (one-way ANOVA, $F_{2,18} = 2.2$, $P = 0.14$), jump (one-way ANOVA, $F_{2,18} = 0.55$, $P = 0.58$), rearing (one-way ANOVA, $F_{2,18} = 0.09$, $P = 0.91$) and latencies (one-way ANOVA for each behaviour, $P > 0.05$). Controls are pooled from saline injected mice. **q**, Tail suspension test. Percentage of time spent struggling. One-way ANOVA, $F_{2,20} = 0.31$, $P = 0.74$. **r**, Social interaction. Interaction time was similar across groups; one-way ANOVA, $F_{2,19} = 0.31$, $P = 0.74$. **s**, Righting reflex for GRIN1-knockout and HCN1-knockout mice.

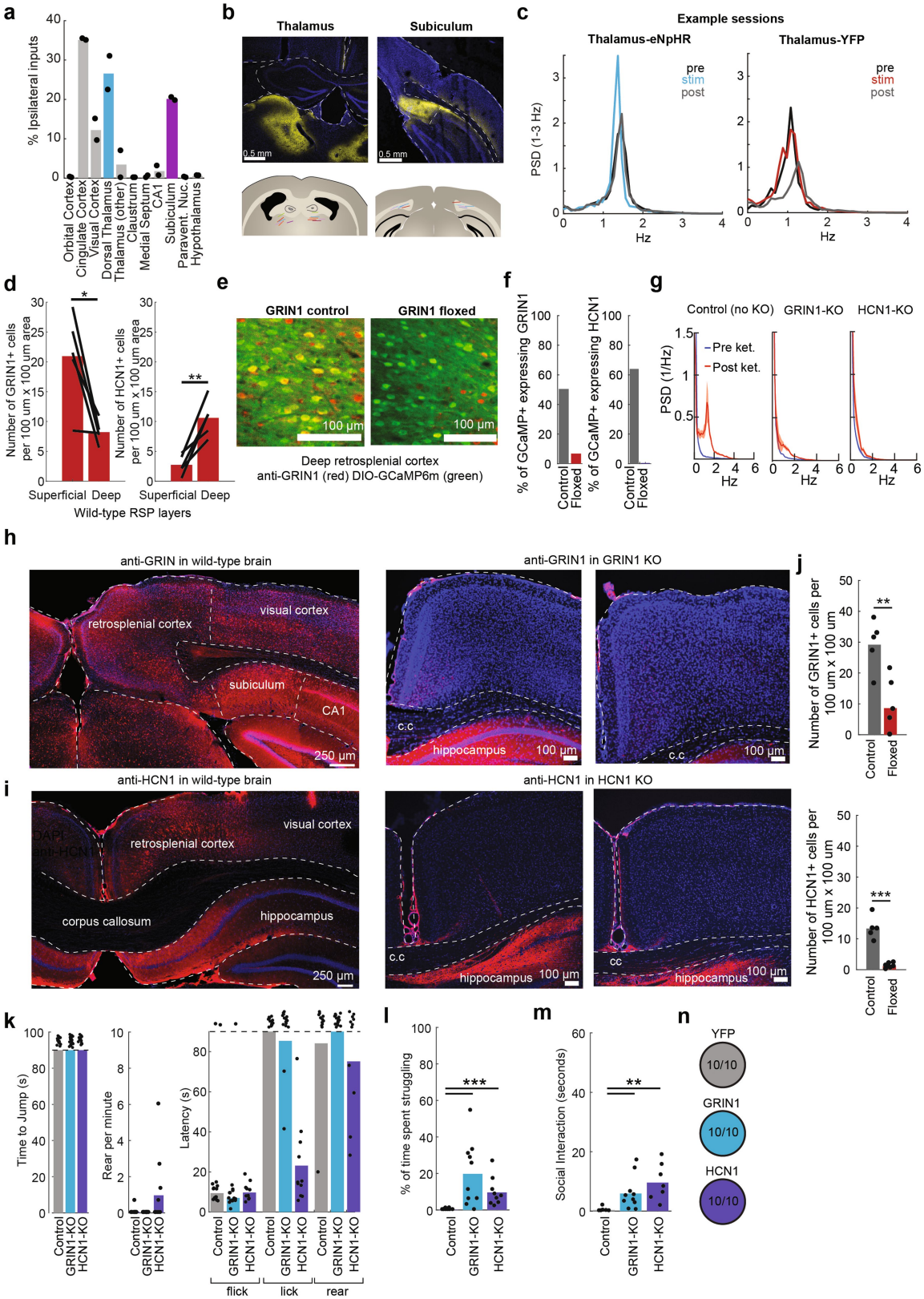

Extended Data Fig. 11 | See next page for caption.

Extended Data Fig. 11 | Additional information for long-range input and gene knockout experiments. a, Percentage of ipsilateral inputs from non-retrosplenial regions across the whole brain ($n = 2$ mice). The bar denotes the mean. **b**, Top, example confocal image showing eNPHR3.0–YFP expression. Bottom, localizations of the fibre tip in opsin-expressing mice, each colour is an individual mouse. Scale bars, 500 µm. **c**, Frequency content of example recording in a dorsal thalamus NpHR3.0 mouse. Each time window (pre, stim, post) consists of 2 min. **d**, Density of GRIN1 (left) and HCN1 (right) cells in the RSP. GRIN1-expressing neurons were more dense in superficial than in deep layers (paired *t*-test, $P = 0.023$; Hedge's $g = -1.94$), but HCN1-expressing neurons were mostly found in deep layers (paired *t*-test, $P = 0.0066$; Hedge's $g = 2.71$). **e**, Confocal images showing expression of AAVdj-Ef1a-DIO-GCaMP6m and GRIN1 in control (left) and GRIN1-floxed (right) deep RSP. **f**, Quantification of gene disruption effectiveness in photometry experiments. Co-localization of GRIN1 and HCN1 with GCaMP6m was greatly reduced. **g**, Quantification of oscillation frequency content (PSD) before (blue) and after (red) ketamine injection, $n = 7$ mice in each group. **h**, Confocal images showing distribution of $GRIN1^+$ neurons in wild-type and GRIN-knockout mice. **i**, Confocal images showing distribution of $HCN1^+$ neurons in wild-type and HCN1-knockout mice. **j**, Quantification of gene disruption for behavioural experiments. Density of $GRIN1^+$ cells (unpaired *t*-test, $P = 0.0031$; Hedge's $g = -2.22$) and $HCN1^+$ cells (unpaired *t*-test, $P < 1 \times 10^{-4}$, Hedge's $g = -4.64$) were significantly reduced by injections of AAVdj-Ef1a-Cre (12 injections per mouse). **k**, Hot-plate test. No mice jumped before the maximum allowable time, indicated by the dashed horizontal line. Rate of rears was not significantly different (corrected Mann–Whitney *U*-test $P > 0.1$) for either group. Average latency to first lick was lower for HCN1-knockout mice. **l**, Tail suspension test. Significantly increased struggling time was observed in HCN1 and GRIN1 mice (corrected Mann–Whitney *U*-test, $^{**}P < 0.001$. Glass's Δ effect sizes = 1.07, 1.13. **m**, Social interaction. Significantly increased social interaction time was observed in HCN1 and GRIN1 mice (corrected Mann–Whitney *U*-test, $^{**}P < 0.01$). Glass's Δ effect sizes = 0.94, 1.39. **n**, Righting reflex, fraction of mice that right. For each group, all mice successfully corrected postural inversion.

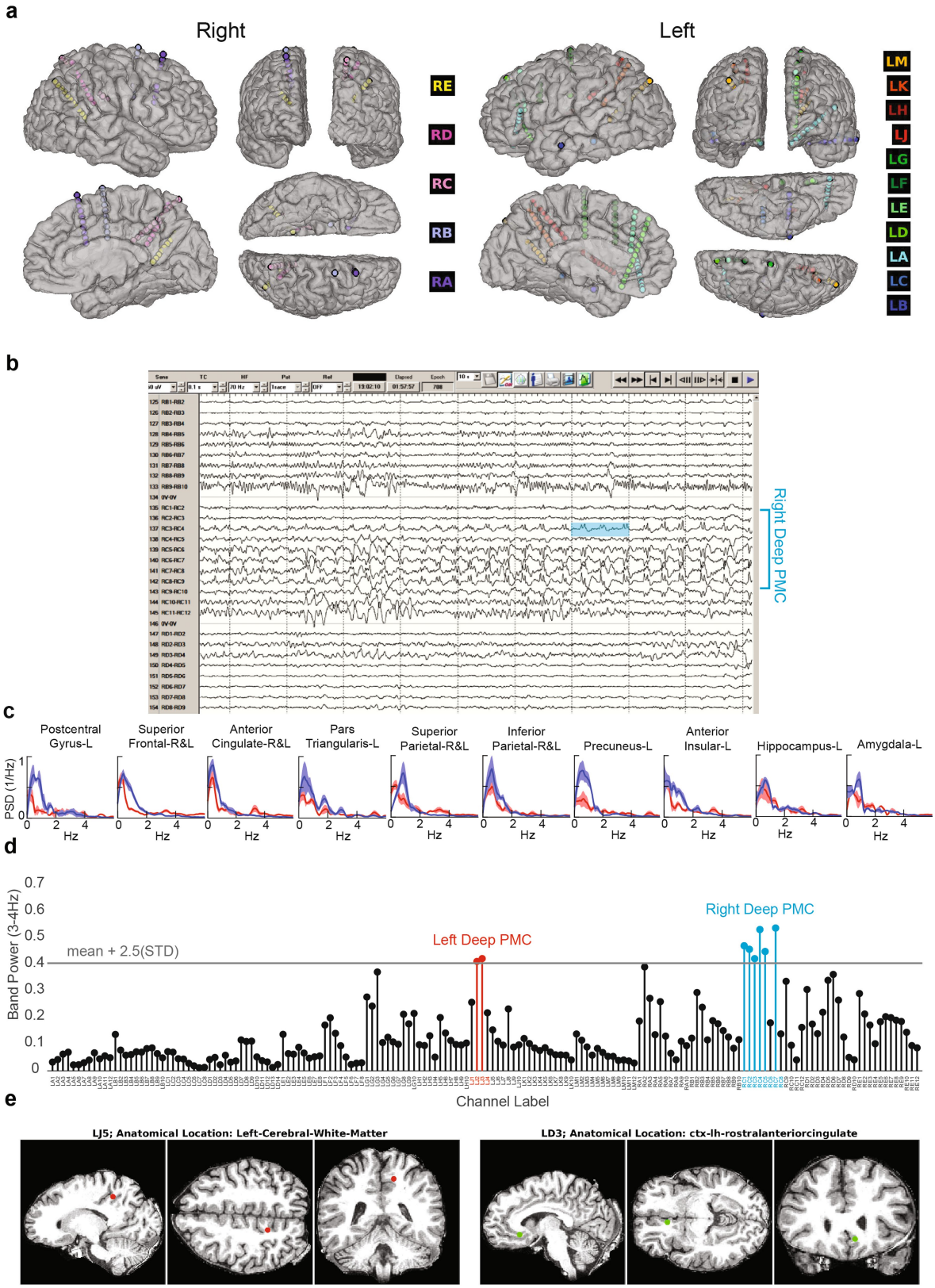

Extended Data Fig. 12 | Additional information on human iEEG recordings. **a**, 3D rendering of electrode locations for right and left hemispheres. **b**, Screenshot of raw clinical iEEG recordings (no processing). The RC electrode is in the right PMC, with RC1 being the deepest contact. Vertical lines are 1 s. Note rhythm in contacts in right deep posteromedial cortex RC3–4 through RC8–9. One second is highlighted in blue showing an approximately 3 Hz rhythm. **c**, Frequency spectrum of iEEG traces from frontal lobe regions, parietal, temporal lobe cortical regions, and subcortical areas during aura (red) or non-seizure (blue) epochs. **d**, Quantification of power in the 3–4 Hz band across all contacts during the seizure aura-period ($n = 2$ seizures, 10 s for each aura). Deep posteromedial regions on both hemispheres exhibit the high power. Contacts that cross threshold (mean + 2.5 × s.d.) are coloured. **e**, Location of electrodes that elicited a dissociative experience (Fig. 5) that were not located in a spontaneously oscillating region of the cortex.

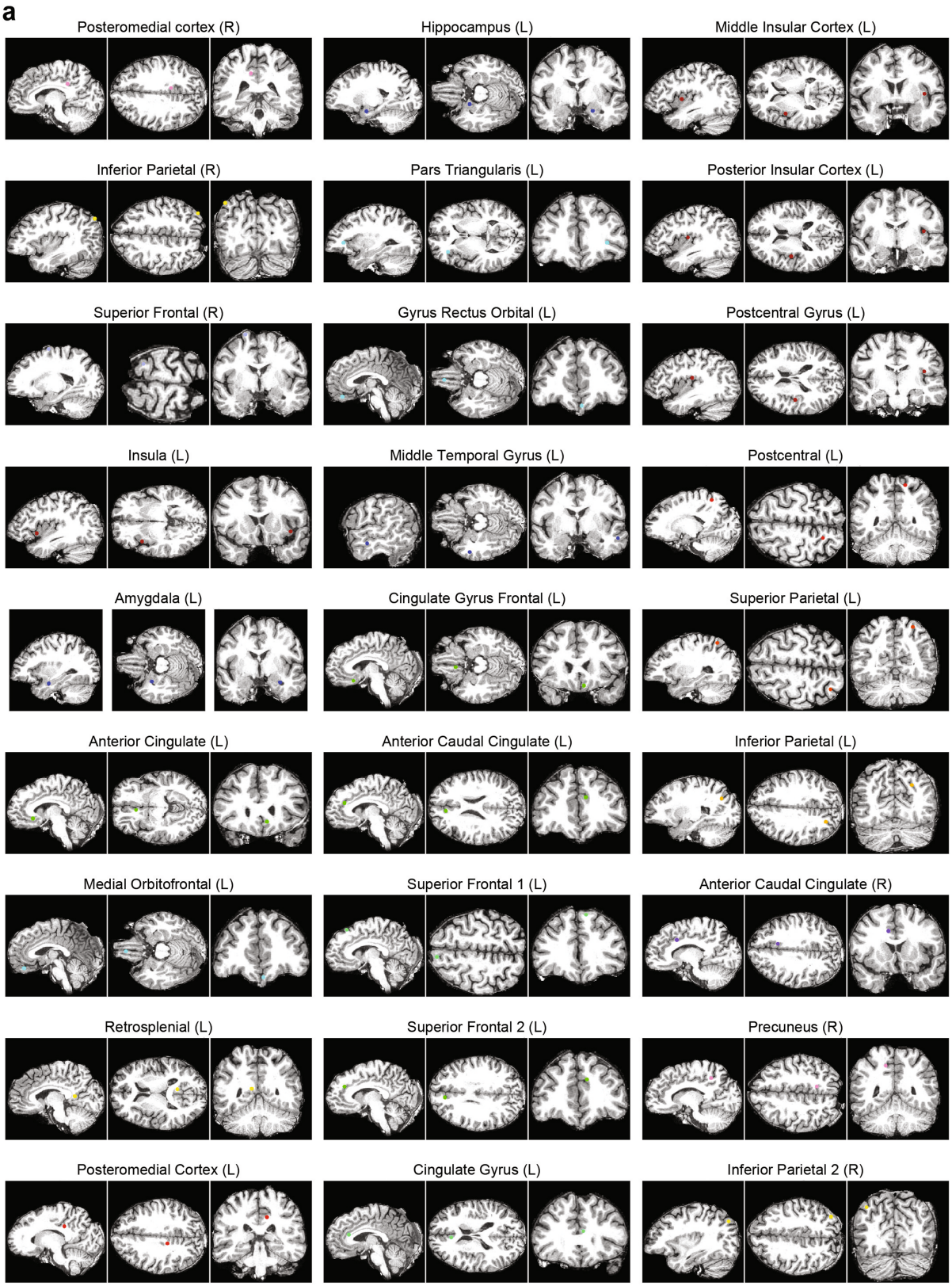

Extended Data Fig. 13 | Locations of electrode contacts for human iEEG recordings. MRI images show anatomical locations of electrode contacts displayed in Fig. 5.

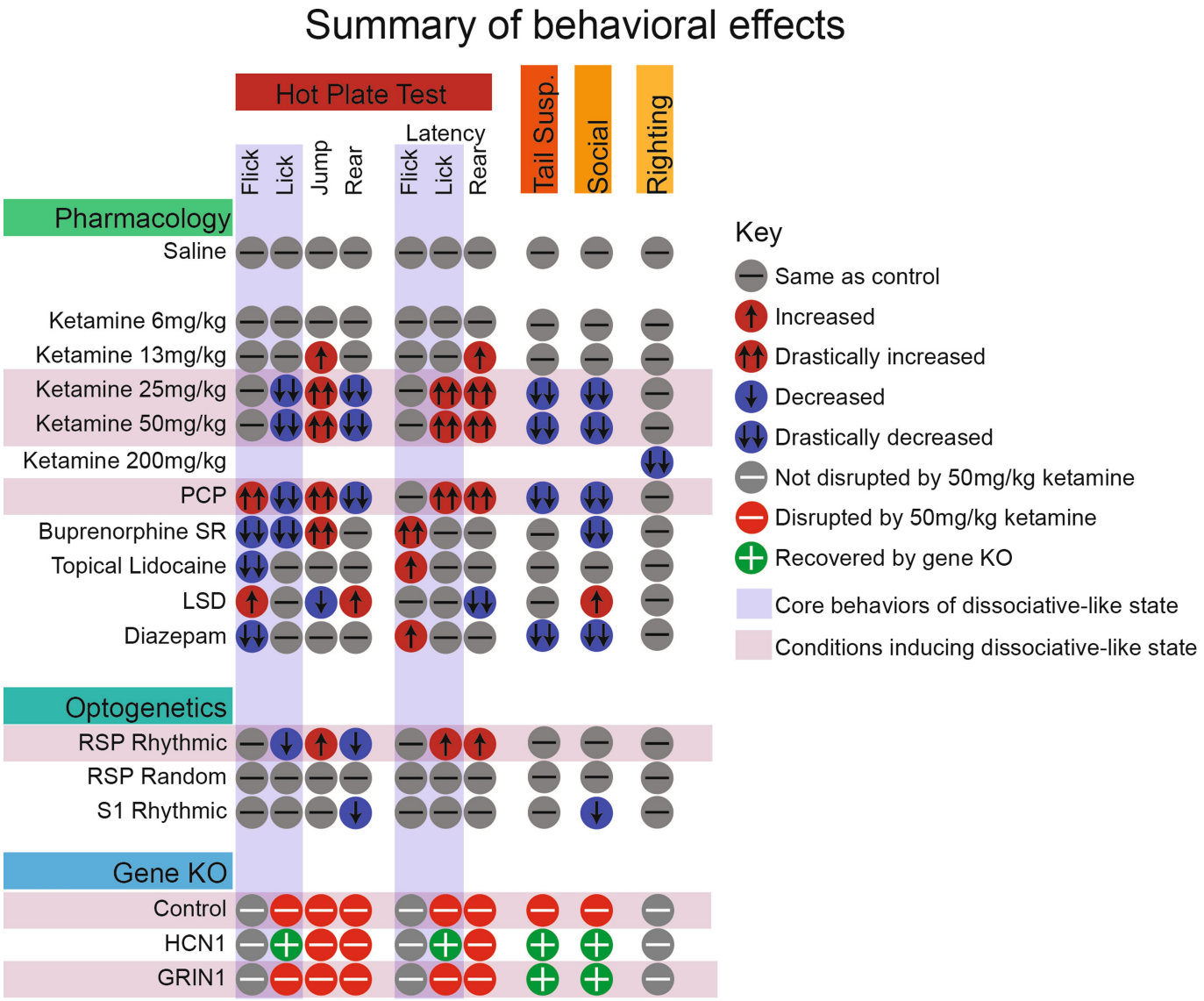

Extended Data Fig. 14 | Summary of behavioural effects in the rodent model. Overview of effects from all rodent behaviour experiments (corresponding to Figs. 3, 4).

nature research

Corresponding author(s): Karl Deisseroth

Last updated by author(s): Jul 23, 2020

Reporting Summary

Nature Research wishes to improve the reproducibility of the work that we publish. This form provides structure for consistency and transparency in reporting. For further information on Nature Research policies, see Authors & Referees and the Editorial Policy Checklist.

Statistics

For all statistical analyses, confirm that the following items are present in the figure legend, table legend, main text, or Methods section.

n/a	Confirmed	
☐	☒	The exact sample size (*n*) for each experimental group/condition, given as a discrete number and unit of measurement
☐	☒	A statement on whether measurements were taken from distinct samples or whether the same sample was measured repeatedly
☐	☒	The statistical test(s) used AND whether they are one- or two-sided *Only common tests should be described solely by name; describe more complex techniques in the Methods section.*
☐	☒	A description of all covariates tested
☐	☒	A description of any assumptions or corrections, such as tests of normality and adjustment for multiple comparisons
☐	☒	A full description of the statistical parameters including central tendency (e.g. means) or other basic estimates (e.g. regression coefficient) AND variation (e.g. standard deviation) or associated estimates of uncertainty (e.g. confidence intervals)
☐	☒	For null hypothesis testing, the test statistic (e.g. *F*, *t*, *r*) with confidence intervals, effect sizes, degrees of freedom and *P* value noted *Give P values as exact values whenever suitable.*
☒	☐	For Bayesian analysis, information on the choice of priors and Markov chain Monte Carlo settings
☒	☐	For hierarchical and complex designs, identification of the appropriate level for tests and full reporting of outcomes
☐	☒	Estimates of effect sizes (e.g. Cohen's *d*, Pearson's *r*), indicating how they were calculated

Our web collection on statistics for biologists contains articles on many of the points above.

Software and code

Policy information about availability of computer code

Data collection	MicroManager v2 for image acquisition, MATLAB >R2016 (Mathworks) for data acquisition, SpikeGLX for Neuropixels
Data analysis	MATLAB >R2016 (Mathworks) for data analysis, Kilosort2 and Phy and Python for Neuropixels processing

For manuscripts utilizing custom algorithms or software that are central to the research but not yet described in published literature, software must be made available to editors/reviewers. We strongly encourage code deposition in a community repository (e.g. GitHub). See the Nature Research guidelines for submitting code & software for further information.

Data

Policy information about availability of data

All manuscripts must include a data availability statement. This statement should provide the following information, where applicable:

- Accession codes, unique identifiers, or web links for publicly available datasets
- A list of figures that have associated raw data
- A description of any restrictions on data availability

The datasets generated and analyzed during the current study are available from the corresponding author on request and at www.optogenetics.org.

Field-specific reporting

Please select the one below that is the best fit for your research. If you are not sure, read the appropriate sections before making your selection.

☒ Life sciences ☐ Behavioural & social sciences ☐ Ecological, evolutionary & environmental sciences

For a reference copy of the document with all sections, see nature.com/documents/nr-reporting-summary-flat.pdf

Life sciences study design

All studies must disclose on these points even when the disclosure is negative.

Sample size	Sample size was chosen using our lab's experience and standards in the field. Power calculations were not made prior to experimentation.
Data exclusions	Criteria for animal exclusion was pre-established. Animals were excluded if injected virus did not express or optical fibers were mis-targeted.
Replication	Gene KO experiments were replicated in an entirely new cohort, and this was the only replication attempt of that experiment. Imaging experiments were replicated across many cohorts and mice. Thalamus inhibition experiments were also replicated successfully in a new cohort.
Randomization	Two sources of randomization were included in this study. First, control and experimental animals were randomly assigned to cages, such that control and experimental animals shared cages. Second, the order of behavioral testing was randomized across groups. For animals that experienced the same test twice, individual animals were counterbalanced within each experimental group.
Blinding	Experimenters were blinded to each animal's group identity while scoring behavioral videos. Experimenters were not blinded to drug identity during imaging experiments.

Reporting for specific materials, systems and methods

We require information from authors about some types of materials, experimental systems and methods used in many studies. Here, indicate whether each material, system or method listed is relevant to your study. If you are not sure if a list item applies to your research, read the appropriate section before selecting a response.

Materials & experimental systems

n/a	Involved in the study
☐	☒ Antibodies
☒	☐ Eukaryotic cell lines
☒	☐ Palaeontology
☐	☒ Animals and other organisms
☒	☐ Human research participants
☐	☒ Clinical data

Methods

n/a	Involved in the study
☒	☐ ChIP-seq
☒	☐ Flow cytometry
☐	☒ MRI-based neuroimaging

Antibodies

Antibodies used	Primary antibodies used: anti-HCN1: 1:500 of abnova MAB6651 lot MH387188, anti-NMDAR: 1:500 of Invitrogen PA5-85751, lot UF2785857C
Validation	anti-HCN1 citations: Congenital long QT syndrome. Crotti L, Celano G, Dagradi F, Schwartz PJ.Orphanet J Rare Dis. 2008 Jul 7;3:18. Ca(V)1.2 calcium channel dysfunction causes a multisystem disorder including arrhythmia and autism. Splawski I, Timothy KW, Sharpe LM, Decher N, Kumar P, Bloise R, Napolitano C, Schwartz PJ, Joseph RM, Condouris K, Tager-Flusberg H, Priori SG, Sanguinetti MC, Keating MT.Cell. 2004 Oct 1;119(1):19-31. anti-NMDAR validation: Example images of primary cortical neurons shown on product webpage (ThermoFisher)

Animals and other organisms

Policy information about studies involving animals; ARRIVE guidelines recommended for reporting animal research

Laboratory animals	Mouse strains used were C57BL/6J (Black 6, Jackson Laboratory, #664), Tg(Thy1-GCaMP6s)GP4.3Dkim (Thy1-GCaMP6s, JAX#024275)41, Cux2-CreERT2 (gift of S. Franco, University of Colorado)20, Ai148(TIT2L-GC6f-ICL-tTA2)-D (Ai148, Jax #030328) (gift of H. Zeng, Allen Institute for Brain Science), Tg(Rbp4-cre)KL100Gsat (Rbp4-Cre, No. 031125-UCD, MMRRC) (gift of L. Luo, Stanford), B6.129S-Hcn1tm1Kndl/J (HCN1f/f Jax #028299) (gift of L. Giocomo, Stanford), B6.129S4-Grin1tm2Stl/J (NR1f/f Jax #005246). Male and female mice were used, aged 6-18 weeks at the time of surgery.
Wild animals	N/A
Field-collected samples	N/A
Ethics oversight	All procedures were in accordance with protocols approved by the Stanford University Institutional Animal Care and Use Committee (IACUC) and guidelines of the National Institutes of Health.

Note that full information on the approval of the study protocol must also be provided in the manuscript.

Clinical data

Policy information about clinical studies

All manuscripts should comply with the ICMJE guidelines for publication of clinical research and a completed CONSORT checklist must be included with all submissions.

Clinical trial registration	N/A
Study protocol	N/A
Data collection	All clinical research was reviewed and approved by the Stanford Institutional Review Board. Informed consent was obtained from the subject prior to participation in the study protocol. The patient (participant number S19-137 / SD056) was implanted with Ad-Tech (Oak Creek, WI) SEEG Depth Electrodes as part of routine Phase II monitoring for refractory epilepsy.
Outcomes	N/A

Magnetic resonance imaging

Experimental design

Design type	*Indicate task or resting state; event-related or block design.*
Design specifications	*Specify the number of blocks, trials or experimental units per session and/or subject, and specify the length of each trial or block (if trials are blocked) and interval between trials.*
Behavioral performance measures	*State number and/or type of variables recorded (e.g. correct button press, response time) and what statistics were used to establish that the subjects were performing the task as expected (e.g. mean, range, and/or standard deviation across subjects).*

Acquisition

Imaging type(s)	*Specify: functional, structural, diffusion, perfusion.*
Field strength	*Specify in Tesla*
Sequence & imaging parameters	*Specify the pulse sequence type (gradient echo, spin echo, etc.), imaging type (EPI, spiral, etc.), field of view, matrix size, slice thickness, orientation and TE/TR/flip angle.*
Area of acquisition	*State whether a whole brain scan was used OR define the area of acquisition, describing how the region was determined.*

Diffusion MRI ☐ Used ☒ Not used

Preprocessing

Preprocessing software	*Provide detail on software version and revision number and on specific parameters (model/functions, brain extraction, segmentation, smoothing kernel size, etc.).*
Normalization	*If data were normalized/standardized, describe the approach(es): specify linear or non-linear and define image types used for transformation OR indicate that data were not normalized and explain rationale for lack of normalization.*
Normalization template	*Describe the template used for normalization/transformation, specifying subject space or group standardized space (e.g. original Talairach, MNI305, ICBM152) OR indicate that the data were not normalized.*
Noise and artifact removal	*Describe your procedure(s) for artifact and structured noise removal, specifying motion parameters, tissue signals and physiological signals (heart rate, respiration).*
Volume censoring	*Define your software and/or method and criteria for volume censoring, and state the extent of such censoring.*

Statistical modeling & inference

Model type and settings	
Effect(s) tested	

Specify type of analysis: ☐ Whole brain ☒ ROI-based ☐ Both

Anatomical location(s)	*Describe how anatomical locations were determined (e.g. specify whether automated labeling algorithms or probabilistic atlases were used).*

Statistic type for inference (See Eklund et al. 2016)	.
Correction	N/A

Models & analysis

n/a	Involved in the study
☒	☐ Functional and/or effective connectivity
☒	☐ Graph analysis
☒	☐ Multivariate modeling or predictive analysis